

RESEARCH

Open Access



Experimental Study on Crack Propagation of Concrete Under Various Loading Rates with Digital Image Correlation Method

Jingwu Bu^{1,2}, Xudong Chen^{3*}, Liangpeng Hu³, Hanqing Yang³ and Saisai Liu³

Abstract

The quantificational exploration of the propagation law of fracture process zone (FPZ) is of great importance to the research on concrete fracture. This paper performed fracture experiments on pre-cracked concrete beams under various loading rates. Digital image correlation (DIC) method was applied to obtain the whole field displacement of concrete in the fracture test. The crack opening displacement (COD) and the evolution of FPZ were determined based on the whole field displacement. The results show that the length of FPZ first increases and then decreases with the development of the effective crack length and the maximum length of FPZ is about 60 mm. It can be found that the length of FPZ corresponding to the peak load decreases with the increase of loading rates. Based on the fictitious crack model, a bilinear softening model was established. According to the proposed model, the mechanical behavior and the propagation law of FPZ were analyzed. The bilinear softening model can reflect the microcrack development and the aggregate interlocking in the FPZ.

Keywords: concrete, loading rates, digital image correlation (DIC), fracture process zone (FPZ), crack opening displacement (COD)

1 Introduction

Most concrete structures in service are subjected to static loads as well as are frequently disturbed by dynamic loads such as earthquakes, shocks and explosions. As a result, studying the effect of loading rates on the fracture mechanical properties is of great practical engineering significance to predicting the crack propagation and failure of concrete structures under dynamic loads, which raised a wide concern in the research field in recent decades (Wang et al. 2016; Al-Osta et al. 2018). Bazant and Gettu (1992) studied the variation of concrete fracture mechanical parameters under different loading rates with size effect model and their results indicated that the fracture toughness, FPZ length and the critical crack opening

displacement increase with the increasing of loading rates. Rosa et al. (2012) conducted three-point bending tests on pre-cracked concrete beams under five loading rates ranging from 1.74×10^{-5} to 17.4 mm/s and found that both the peak load and the fracture energy of concrete increase with the increasing of loading rates. Vidya Sagar and Rao (2014) investigated the influence of loading rates on acoustic emission characteristic parameters obtained in the fracture procedure of reinforced concrete beams with acoustic emission techniques. It was found that as the loading rate increased, the brittleness is more evident and the acoustic emission characteristic parameter (b-value) becomes smaller. To produce low and high strain rates respectively, Zhang et al. (2015) utilized the servo hydraulic testing machine and the drop hammer to perform fracture tests on reinforced concrete beams. Test results showed that the effect of loading rates on crack propagation rate is relatively evident and the crack propagation rate at the initial loading stage remains

*Correspondence: cxdong1985@hotmail.com

³ College of Civil and Transportation Engineering, Hohai University, Nanjing 210098, People's Republic of China
Full list of author information is available at the end of the article
Journal information: ISSN 1976-0485 / eISSN 2234-1315

almost unchanged when the loading rate is comparatively fast, although the propagation rate of the main crack gradually decreases. Hu et al. (2015) performed splitting tensile tests on pre-cracked concrete cubes under four different strain rates (10^{-5} mm/s to 10^{-2} mm/s) and analyzed the influence of loading rates on concrete fracture parameters based on the double-K fracture theory. The testing results indicated that the initial fracture toughness increases linearly but the unstable fracture toughness first increases and then stays unchanged with the increase of loading rates. Meng et al. (2017) studied the influence of loading rates and initial crack-depth ratios on the fracture mechanical properties of ultra-high performance concrete. It was found that the peak load of concrete specimen increases with the increasing of loading rates and the increase amplitude is influenced by the initial crack-depth ratios. It can be concluded that although the influence of loading rates on concrete fracture properties is highly concerned by international scholars, the researches mainly focus on fracture characteristics, e.g. peak loads, fracture toughness, and ignore crack propagation when considering the effect of loading rates. What's more, no consistent conclusions about the relationship between concrete fracture parameters and loading rates have been drawn until now. It makes conducting concrete fracture tests under different loading rates is of theoretical and engineered significance.

Researches on concrete fracture properties indicate that evident strain concentration area, named fracture process zone (FPZ), is located in the crack tip. Phenomena such as microcracks, aggregate interlocking, contact of coarse surfaces and friction all exist in the area (Hillerborg et al. 1976). The FPZ is not only an important characteristic of concrete fracture, but also the fundamental cause of it. In order to describe the relationship of stress and crack opening displacement in FPZ, Hillerborg et al. (1976) proposed a cohesive crack model, which can effectively reflect the softening properties of concrete. Additionally, the model parameters can be determined by fracture tests and it makes this model quite practical. With the further study of FPZ, large quantities of observing techniques and methods have been proposed. The common measuring methods include scanning electron microscope (Krstulovicpara 1993), X-ray technique (Otsuka and Date 2000), laser speckle photography (Ansari 1989) and acoustic emission method (Fathima and Kishen 2015; Haneef et al. 2016). Digital image correlation (DIC), which is a combination of the modern digital image processing technology and optical measurement mechanics, is a new optical method invented in 1980s. By comparing the speckle patterns during the loading procedure of specimens, the deformation of the observing area can be calculated (Fu and He 2010). Since the nature of the technology is non-interference, drawbacks of many traditional

optical measurements can be effectively avoided and the advancement has made a wide application in the deformation measurement of quasi-brittle materials such as concrete and rock in recent years. Wu et al. (2011) studied the influence of specimen size on the development of concrete FPZ with DIC method and found that the FPZ length at the moment that it is most fully developed increases with the increase of specimen height, but decreases with the increase of initial crack-depth ratios. Dong et al. (2017) further extended the research by Wu et al. (2011) and studied the development of the FPZ of concrete beams under complex fracture mode. Gajewski and Garbowski (2014) determined the fracture mechanical parameters of concrete by combining DIC technique with inverse analysis. Skarzynski et al. (2011) focused on researching the shape and width variations of FPZ of concrete beams in the fracture procedure by DIC technique and investigated the influence of characteristic length and aggregate size on FPZ length. Asmaro (2013) conducted wedge splitting tests on concrete specimens of different ages and analyzed the FPZ development in quantification by DIC technique. All the previous researches shown above demonstrated that it is available to study the crack propagation and nonlinear fracture mechanism of concrete by utilizing DIC.

Since the three-point bending test is recommended as a standard method to study the mode I crack by RILEM (1990), three-point bending tests on pre-cracked concrete specimens under different loading rates with MTS 322 device are performed and crack propagation is investigated by using DIC method. Based on the measurements recorded in the fracture procedure, the whole field displacement and FPZ development were analyzed.

2 Test Program

2.1 Three-Point Bending Test

The mix proportion used in the study is shown in Table 1. Ordinary Portland cement of grade 42.5, river sand with particle size distribution fitting ASTM C33/C33M-18 (2018), aggregates with maximum size of 20 mm and water were used in casting of concrete. The concrete mixture was casted into 100 mm × 100 mm × 400 mm moulds and demoulding was taken after 24 h. Then the specimens were cured in water for 28 days. Before the experiment, a pre-crack with a depth of 30 mm was cut along the height in middle of the specimen and water was used to wash away

Table 1 Mix proportions of concrete.

Water (kg/m ³)	Cement (kg/m ³)	Sand (kg/m ³)	Aggregate (kg/m ³)	Water/cement	Sand ratio (%)
175	461	511	1253	0.38	0.29

the ashes and pastes inside the cracks. In the procedure of the experiment, the specimens were put on the supports with the cracks facing downward and the distance between two supports was kept as 300 mm. The loader was located above the middle of the specimens and faced with the pre-crack. In this study, a hydraulic servo closed-loop testing machine (MTS 322) was used to conduct the three-point bending tests on concrete specimens. The load was recorded by the load sensor in the machine and then saved by the computer while the crack mouth opening displacement (CMOD) was measured by using the clip-on extensometer. In order to obtain the post-peak region of the stress–strain curve, CMOD was used to control the loading process and the loading rates were set as 0.001 mm/s, 0.01 mm/s and 0.1 mm/s to investigate the effect of loading rates on monotonic fracture properties of concrete. The three-point loading method is shown in in Fig. 1.

2.2 DIC Test

Before DIC test, a specimen surface with less pores and flaws was selected for measuring. The ashes were cleared away by a brush and the measurement area (the extended area of FPZ) was repeatedly sprayed with matte black paint. Then the camera tripod and slide were installed. By adjusting the position of the camera tripod and the slide, the image acquisition area was aimed and the camera lens surface was kept parallel to the surface of the specimen. Afterwards, the image was optimized to the clearest by adjusting the focus of the lens and the lighting equipment was put in place with lighting adjusted. After all the adjustments were finished, the MTS 322 was started and the load was applied, during which the images were collected by the



Fig. 1 Three-point bending fracture test of concrete.

high-speed camera and the frequency of image collection was 2 images/s.

3 Fracture Mechanical Properties of Concrete Under Three-Point Bending

3.1 P-CMOD Curve Obtained by Traditional Method

Figure 2 shows the monotonic load-crack mouth opening displacement (P-CMOD) curves of concrete under three different loading rates by using the traditional clip-on extensometer. It can be seen that the P-CMOD curve is approximately linear before peak load and is nonlinear near the peak load, while after the peak load it presents evident softening phenomenon. It can also be seen that with the increasing of loading rates, concrete peak load goes up. It indicates that concrete has significant loading rate effect on fracture. However, in terms of displacement, under the circumstances of three loading rates, the peak CMODs of concrete are 0.028 mm, 0.041 mm and 0.038 mm, where the loading rate effect is not obvious. All the details of the experimental specimens are show in Table 2.

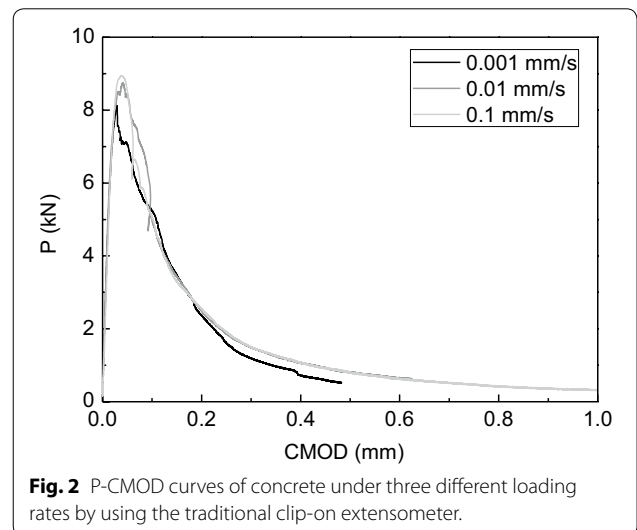


Fig. 2 P-CMOD curves of concrete under three different loading rates by using the traditional clip-on extensometer.

Table 2 The details of the experimental specimens.

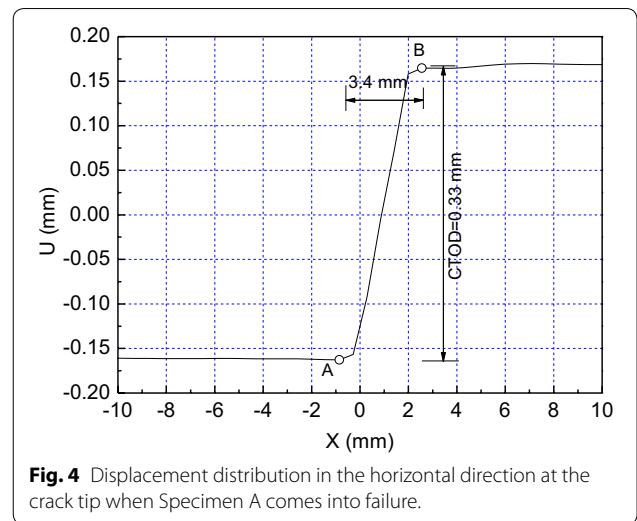
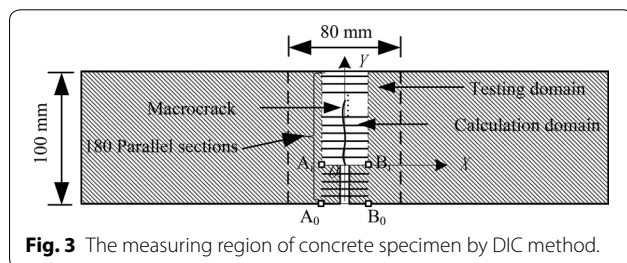
Serial number	Loading rate (mm/s)	f_c (MPa)	P_{peak} (kN)	$CMOD_{peak}$ (mm)
Specimen A	0.001	62	8.12	0.028
Specimen B	0.01		8.75	0.041
Specimen C	0.1		8.94	0.038

3.2 P-CMOD Curve Obtained by DIC Method

3.2.1 Determination Method of Crack Opening Displacement

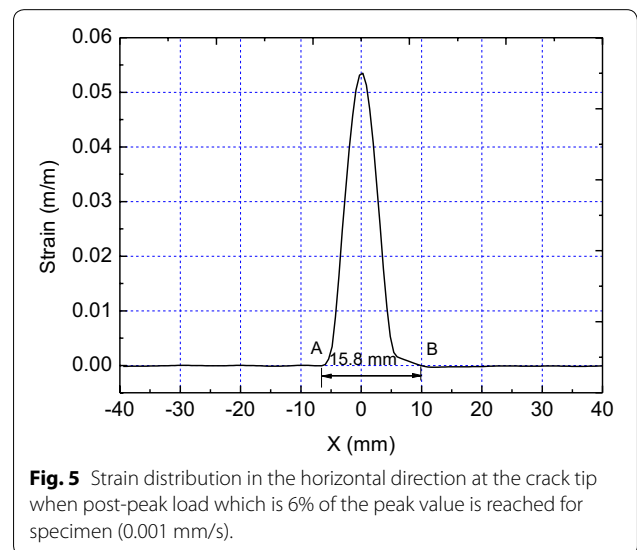
The dimension of the measuring domain used in the study is 100 mm × 80 mm and is large enough to cover the initial crack, crack tip and the whole area of the effective height. The detailed dimensions are shown in Fig. 3.

In the study, the relative coordinate method was used to calculate the displacement difference to determine the crack opening displacement. The specific method is shown as follows: The measurement area was divided into 180 parallel sections along the direction of crack propagation as shown in Fig. 3. In order to ensure that the calculating width on each section contains the whole FPZ, the width of each cross section was 20 mm and by this method the crack opening displacement of each section along the direction of crack propagation could be calculated after determining the area of the testing region. For instance, to calculate the crack tip opening displacement (CTOD), the variation of displacement along the calculating width of the section should be firstly obtained. Figure 4 shows the variation process of the displacement on the horizontal section where the initial crack tip is located when the specimen is failure. It can be seen that the displacement on the left side of the crack is negative while on the right side is positive. A sudden displacement change happened within the crack in the direction perpendicular to crack propagation, which caused stress concentration and the crack propagation. The width of FPZ at the position is the distance between two points where sudden displacement change occurs. For example, in Fig. 4, the distance between A and B in the X direction is about 3.4 mm, while the CTOD is 0.33 mm, which is the displacement difference between A and B. As a result, the COD at each section along the height direction of the specimen is the displacement difference between two points where sudden displacement change occurs in the width range. Parallel sections are selected from the specimen bottom along the direction of crack propagation and then the horizontal displacement distributions in the parallel sections can be obtained. In this way, the variation of the whole FPZ width with height can be determined and the actual distribution of the whole FPZ can be described, which provides reliable experiment data for



the analysis of the nonlinear fracture mechanical properties of concrete. Since only mode I crack was studied in this paper and the vertical deformation was small, the deformation in the vertical direction was ignored when calculating COD of each section.

In addition, according to the strain cloud chart in the measurement area of specimen obtained by DIC method, strain distribution on line AB in the cross section at the crack tip when Specimen A comes into failure can be described, as shown in Fig. 5. It can be seen that a significant strain concentration is generated between - 5.9 and 9.9 mm, and the width of the strain concentration area is 15.8 mm in the direction perpendicular to the crack propagation. It can also be found that the width of strain



concentration is wider than that of crack expansion, for which the reason may be explained that crack generates when the strain exceeds the maximal value and concrete can be assumed as elastic before the value is reached.

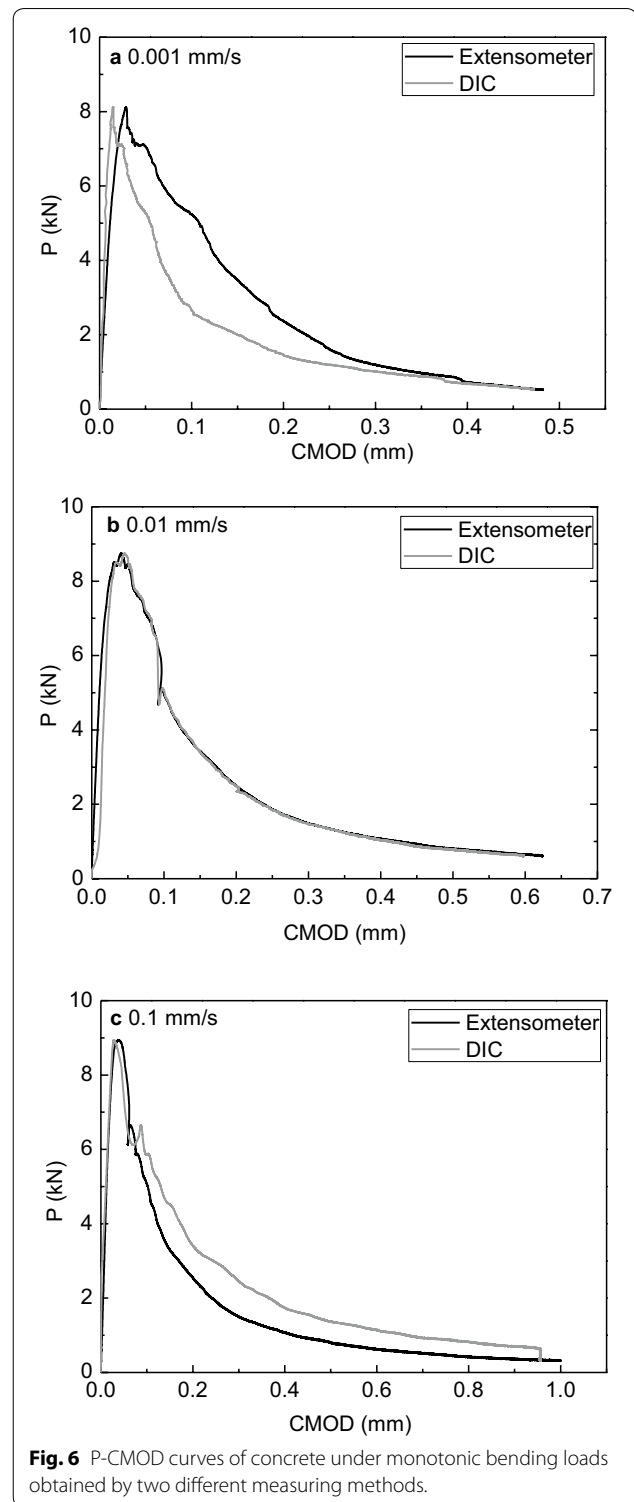
3.2.2 CMOD

To determine CMOD by DIC method, only the COD at the location $Y = -30$ mm needs to be calculated. The photographing speed is 2 frames/s in this experiment. According to the record of COD with the process of photographing, the variation law of CMOD and P-CMOD curve can be obtained.

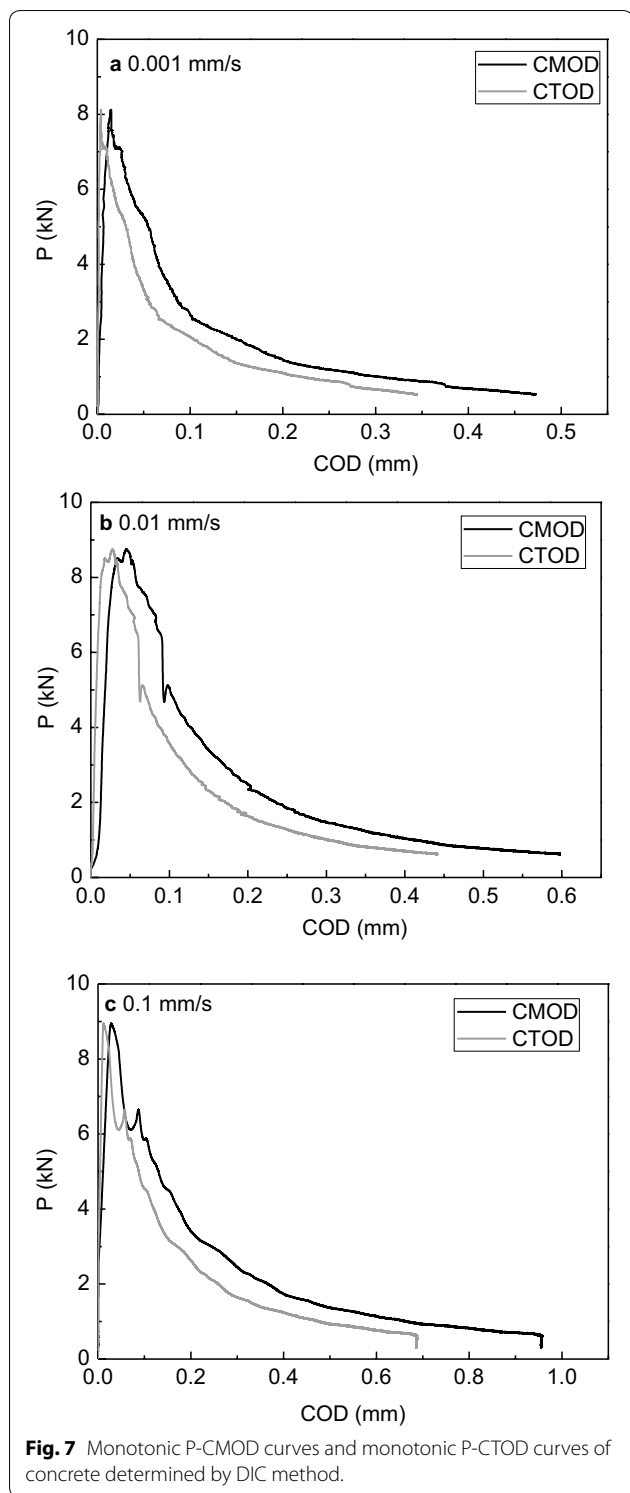
In order to verify the reliability of DIC method, the CMOD obtained by DIC is compared with the result recorded by the traditional one with the clip-on extensometer. Figure 6 indicates the monotonic P-CMOD curves of concrete calculated by both DIC method and clip-on extensometer method under different loading rates. Although some certain deviations can be observed in the experimental curves obtained by the two methods, the curves almost coincide with each other on the whole, which demonstrates the reliability of DIC method to measure the fracture mechanical properties of concrete. The reasons for the difference may be explained as follows: Firstly, since DIC and MTS machine are two independent systems, at present the two systems can not completely simultaneously collect data. Instead, manual start of photographing was adopted in the study at the moment that the loading process of MTS machine began and the method unavoidably contributed to time differences between the two systems. Secondly, the clip-on extensometer was fixed on the mouth of the pre-cut crack, any small accidental displacement at the clip-on edge could affect the experimental results in the loading process. Thirdly, the image collecting frequency of DIC experiment was much smaller than that of the MTS machine, which may influence the accuracy of the experimental results, and especially after the peak load when the loading capacity decreased rapidly, it may lead to some relatively large errors.

3.2.3 CTOD

The traditional clip-on extensometer can effectively obtain the variation of CMOD, but have difficulty in getting the values of CTOD. In comparison, as a non-contact nondestructive testing method, DIC method can measure the whole field displacement of the targeted area. In this study, DIC method was used to obtain the CTODs of concrete specimens. In order to intuitively compare the differences between CMOD and CTOD, both values obtained from the same specimen are depicted in Fig. 7. In the figure, COD on the abscissa represents the crack opening displacement at any location, CMOD represents



crack mouth opening displacement, and CTOD represents crack tip opening displacement. It can be seen that the shape of P-CTOD curve is almost the same as that of



P-CMOD curve and the former value is a bit smaller than that of CMOD on the same condition.

No microcracks emerge in concrete materials when concrete is loaded less than 40% of the peak load. On that

stage, the P-CMOD curve is almost linear. As a result, the stage can be regarded as linear elastic and the difference between CMOD and CTOD is comparatively small. When the load exceeds proportionality limit, the difference becomes larger with the increase of load. To be more specific, the deviation between the two P-COD curves is mainly caused by the differences of measuring locations. With the propagation of cracks, the rotation angle formed between the crack mouth and the crack tip gradually increases, which also leads to the increase of the difference of CODs. Looking back to the linear stage, because the values of COD are comparatively small, the influence of the rotation angle on CODs of two different locations is not evident.

Although certain deviations exist in the COD values obtained by the two different measuring methods, both results are valid for crack measurement of concrete materials. Since DIC method can get the whole field displacement of concrete specimens, it is very convenient to analyze the development of concrete FPZ by the measuring method. Besides, two other advantages can be drawn as follows: As a non-contact measuring technique, the measuring range is not influenced by the distance of the measuring apparatus. Secondly, the measuring procedure is not disturbed by the vibration and noise of the loading equipment, which makes the testing error much smaller than that of traditional method.

4 Fracture Process Zone (FPZ)

4.1 The Formation of FPZ

The fracture of concrete is a phenomenon of slow crack propagation, which can be seen as time-dependent. In the zone at the crack tip, the process of stress relief exists. However, due to the interlocking between aggregates and mortars, the zone is still able to withstand parts of the stress and it can be named as strain softening phenomenon, which is the main cause of the inapplicability of linear elastic fracture mechanics to the study of fracture properties of concrete materials. As a result, inspired by the classical model of elastoplastic mechanics, Hillerborg et al. (1976) proposed fictitious crack model, which can reflect the softening effect, and introduced the conception of FPZ. FPZ is the stress concentration area existing at the crack tip when concrete structures with cracks bear external loads. Although large amounts of microcracks emerge in FPZ, the interlocking between aggregates has bridging effect and it makes the FPZ is still able to transfer partial stress. With the continuous increase of the applied load, the length of FPZ gradually develops and the CODs at the fracture surface also increase. The macrocracks emerge and propagate when the CTOD exceeds the critical value. At the same time, FPZ continues to develop and the cohesive stress in FPZ continuously

redistributes with the process of mechanical loading. The stress never exceeds the tensile strength of the material since there is no stress singularity at the crack tip. When the stress intensity factor generated by external load exceeds that of cohesive stress in FPZ, the concrete structure cannot bear larger loads and the load at the moment is equal to the maximal value. The crack and FPZ can propagate continuously if displacement control is used to conduct the loading process. The capacity of concrete gradually decreases and the macroscopic mechanical response of concrete goes into the softening stage since the concrete structure cannot sustain larger load. In the whole loading process of concrete, the boundary between the macrocrack and FPZ depends on whether the CTOD exceeds the critical value and whether the strain exceeds the peak strain. The peak strain of concrete is the value corresponding to the peak stress in the stress–strain curve of concrete. Based on the experimental results from reference (Chen et al. 2017), the peak tensile strain of concrete at the loading strain of $10^{-6}/s$ is $123 \mu\epsilon$. When the CTOD is smaller than the critical value, the length of FPZ is from the initial crack tip to the location of maximum strain (the tip of the new crack). When the CTOD exceeds the critical value, the length of FPZ is from the new crack tip to the location of maximum strain. During the procedure, with the process of external loading, the location of new crack tip propagates continuously.

It can be seen from the above analysis that the difficulties of describing the fracture properties of concrete can be described as the several points like the complicity of the crack propagation path, the location determination of the crack tip, the size of FPZ, and etc. Therefore, apart from the necessity of researching the variation of CMOD and CTOD, parameters of macroscopic fracture mechanics such as the crack propagation path, the location of crack tip, the length of FPZ and the dissipative energy of crack propagation also need to be studied. DIC method can directly measure the whole field displacement, the crack propagation law and the development of FPZ.

Figure 8 indicates the P-CMOD curve obtained by the traditional clip-on extensometer when testing the pre-cracked concrete beam specimen under the loading rate of 0.001 mm/s. The points on the curve represents different loading stages which need to be studied. Figure 9 shows the strain fields of concrete specimen by using DIC method on various stages, which corresponds to the points on the P-CMOD curve shown in Fig. 8. Figure 9a indicates the strain field distribution in the measurement area when 70% of the peak load is reached in the post-peak region. It can be seen that large quantities of strain concentration areas distribute randomly on the specimen surface, including the areas near the initial crack tip. The main reason for the phenomenon can be concluded

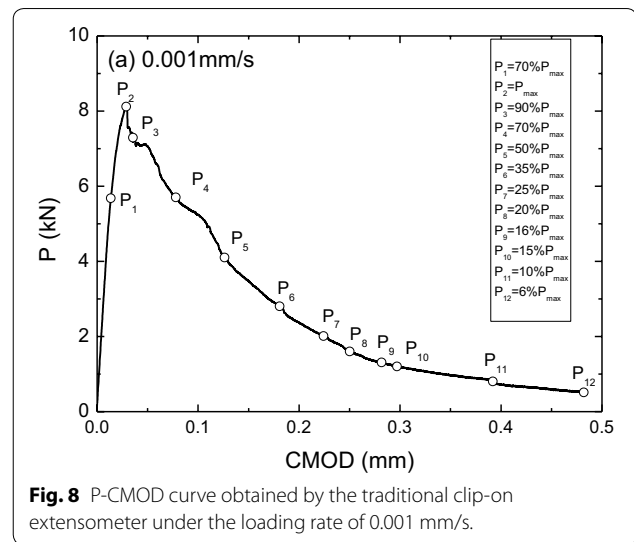


Fig. 8 P-CMOD curve obtained by the traditional clip-on extensometer under the loading rate of 0.001 mm/s.

as follows. Since concrete is a heterogeneous material, large numbers of initial flaws, including pores, microcracks, etc., can generate in the casting and curing procedures and stress concentration is very likely to take place in these areas. With the increasing of load to the peak value, the distributed strain concentration areas decrease gradually and gather towards the new crack tip, where the microcracks accumulate continuously, as shown in Fig. 9b.

The P-CMOD response of concrete gradually becomes softening under the continuous load. At the moment, the microcracks at the crack tip continue to aggregate and the strain in other places is further released, together with the decrease of secondary cracks and the formation of FPZ with certain width along the direction of the initial crack, just as shown in Fig. 9c. Then the development of FPZ starts to accelerate. By comparing Fig. 9c, d, it can be seen that the secondary cracks disappear rapidly and the stress concentration area at the crack tip becomes more evident. Moreover, after the release of strain in other places, only a small residual strain with the value of 5.5×10^{-5} is remained. At the end of the stage, the secondary cracks disappear completely and a major crack forms at the initial crack tip. As a result, the failure characteristics of concrete can be concluded as follows, before the formation of the major crack, random microcracks emerge in the whole range of the specimen. Then after the major crack forms, the stress of other sections gradually releases and the major crack continues to propagate. After the loading stage, the propagating path of the major crack is very clear and constantly develops along the major crack in the following loading procedure. However, at several initial loading stages of the formation of the major crack, such as P_5 and P_6 in Fig. 9e, f, parts of

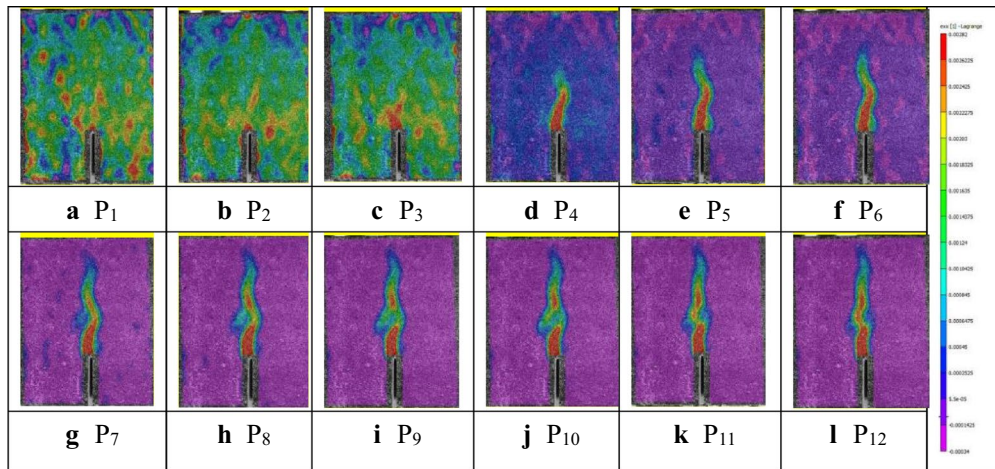


Fig. 9 The strain fields of concrete specimen on different loading stages by using DIC method (0.001 mm/s).

the residual stress in other sections are not fully released and little strain can still be observed despite the fact that the major crack has formed. Only when it reaches stage P_7 stress in the sections outside the major crack is almost completely released with the remaining strain approaching the value of 0. When the FPZ is fully developed, the strain outside FPZ decreases and the corresponding sections gradually turn into traction-free area. To be more specific, the traction-free area forms at 16% of the peak load in the post-peak region and can be observed on stage P_9 , as shown in Fig. 9i. On stage P_9 , the length of the effective crack and FPZ are 89.94 mm and 59.94 mm respectively and the CTOD is 0.155 mm. The detailed analysis can be seen in the following sections.

4.2 The Determination of FPZ Length

The precise measurement of FPZ length plays an important role in predicting the concrete structures failure and selecting the proper specimen size. For concrete materials, due to the interlocking of aggregates and the variation of crack propagating paths, one of the difficulties in the development of concrete FPZ is how to accurately determine the locations of the major crack and the new crack tip. According to the definition of FPZ, to obtain its size, the critical COD first needs to be determined and then whether the material is completely cracked can be judged. According to the cohesive crack model, the stress distribution of concrete in FPZ is the function of COD ($\sigma = f(w)$) with the critical crack opening displacement w_0 as one of the main parameters of the function. To determine the model parameters, the model form needs to be firstly determined. According to the study by Peterson (1981), the relationship between COD and stress can be represented by the bilinear model. The parameters of

the model include the tensile strength of concrete f_t , the turning point stress σ_1 , the crack opening displacement w_1 , and the critical crack opening displacement w_0 . In the study, the tensile strength obtained from the research by Chen et al. (2017) can be used and the value is 4.16 MPa. The determination of the critical crack opening displacement w_0 is dependent on the concrete fracture energy (G_f) which can be determined by the area under the load-loading point displacement ($P-\delta$) curve to the area of the fracture surface under three-point bending loads. However, since the displacement of the loading point is easily affected by its plastic deformation and that of the supports, the measuring errors are comparatively large, which results in large fluctuation in the calculated fracture energy (Zhu 2011). Compared to the displacement of the loading point, CMOD can be conveniently measured by the clip-on extensometer. The fracture energy of concrete can be indirectly calculated based on P-CMOD relationship under three-point bending tests using the equations deduced by Zhang and Xu (2008). Meanwhile, from the results in reference (Zhu 2011), by comparing the fracture energy determined by P-CMOD curve shown in the study by Zhang and Xu (2008) and that calculated by the method recommended by RILEM, both the calculating results are close to each other and the calculating result by Zhang and Xu (2008) is more stable. Lee and Lopez (2014) investigated the fracture energy by using two loading conditions: constant stroke control and constant CMOD control. Test results showed that a far tail constant “A” could change the true fracture energy by up to 11% by using P-CMOD instead of P- δ . What's more, Asmaro (2013) found that the fracture energy calculated by P- δ curve is 1.1 times of that obtained by P-CMOD curve. The above researches all indicate that

it is feasible to calculate the concrete fracture energy by P-CMOD curve. To simplify the calculation, the proportion of the area enclosed by P-CMOD curve to the fracture surface area is used and multiplied by the experience coefficient of 1.1 to determine the fracture energy of concrete. In terms of the determination of σ_1 , many researchers have paid attention to it. Since the bilinear model can effectively simulate the softening properties of concrete FPZ, Wittmann et al. (1990) established a concrete softening constitutive model on the basis of it and found that σ_1/f_t for plain concrete is commonly less than 0.25. Asmaro (2013) conducted mode I fracture tests on plain concrete and applied the bilinear softening model to the material by inverse analysis. The results showed that σ_1/f_t is within the range between 0.4 and 0.53. Huang (2016) obtained the numerical solution of the softening curve based on the cohesive crack model, where the values of σ_1/f_t and w_1/w_0 are 0.25 and 0.4 respectively. In the study, based on the bilinear softening model established by Hillerborg et al. (1976), the value of 3 is taken as σ_1/f_t and w_1 is calculated by the ratio of $0.8G_f$ to f_t ($w_1 = 0.8G_f/f_t$). Because the mix proportions, the loading modes and the calculating methods are different in the above studies, the obtained model parameters would be different. Since the Hillerborg's model is both moderate and widely applied, in the study it is used to determine the model parameters with the calculating method of $w_0 = 3.6G_f/f_t$. The softening model parameters of FPZ under different loading rates are shown in Table 3.

According to the strain field distribution and the COD distribution with the specimen height obtained by DIC method, the sizes of FPZ and the macrocrack can be determined. The specific method is shown as follows, at the beginning of the FPZ, the COD reaches its critical value while at the end side, the strain reaches its maximum value. Therefore, the end of the FPZ is firstly determined based on the strain field distribution of concrete. At the initial loading stage, the COD at the

tip of the macrocrack is smaller than the critical value ($CTOD \leq CTOD_c$). At that time, FPZ includes the area from the tip of the macrocrack to the location where maximum strain is reached. With the process of mechanical loading, the COD at the crack tip gradually increases. When the critical value is exceeded ($CTOD > CTOD_c$), the FPZ is the areas between the points of the critical value and the maximum strain.

In this study, fracture tests of concrete specimens are carried out under monotonic three-point bending loading at various loading rates. Specific methods to determine the length of FPZ of concrete beams with pre-cut notches are given in the following sections.

4.2.1 Specimen A (0.001 mm/s)

In the test, a high-speed camera is used to take images of concrete during the fracture tests and failure images of the whole loading process are obtained. The COD calculation method mentioned in the previous section is used to post-process each image, by which the variation curves of COD with the loading process can be obtained. Figure 10 shows the variation curves of COD at several sections of specimen A. It can be seen from the figure that the COD at each section increases gradually with the mechanical loading process.

Figure 11 shows the FPZs and COD distributions of specimen A at the typical loading stages. When 70% of the peak load is reached in the pre-peak region, the CTOD is 0.0025 mm, which is less than the $CTOD_c$, and no macroscopic crack is formed at that time. Besides, the length of FPZ is 5.18 mm, which is 0.074 times of the effective height (70 mm). When the peak load is reached, CTOD is 0.0062 mm, which is still smaller than the critical value, and the macrocrack is still not able to be observed. At that time, the length of FPZ is 6.46 mm, which is 0.092 times of the effective length. When the specimen is loaded to 90% of the peak strength in the post-peak region, CTOD is 0.0076 mm and still smaller

Table 3 Fracture parameters of concrete under different loading rates.

Softening model	Loading rate (mm/s)	G_f (N/mm)	f_t (MPa)	σ_1 (MPa)	w_1 (mm)	w_0 (mm)
Hillerborg model	0.001	0.182	4.12	1.37	0.035	0.159
	0.01	0.220	4.24	1.41	0.042	0.187
	0.1	0.238	4.56	1.52	0.042	0.188
CEB model (1990)	0.001	0.182	4.12	0.62	0.045	0.287
	0.01	0.220	4.24	0.64	0.053	0.337
	0.1	0.238	4.56	0.68	0.053	0.339
CEB model (2010)	0.001	0.182	4.12	0.82	0.044	0.221
	0.01	0.220	4.24	0.85	0.052	0.259
	0.1	0.238	4.56	0.91	0.052	0.261

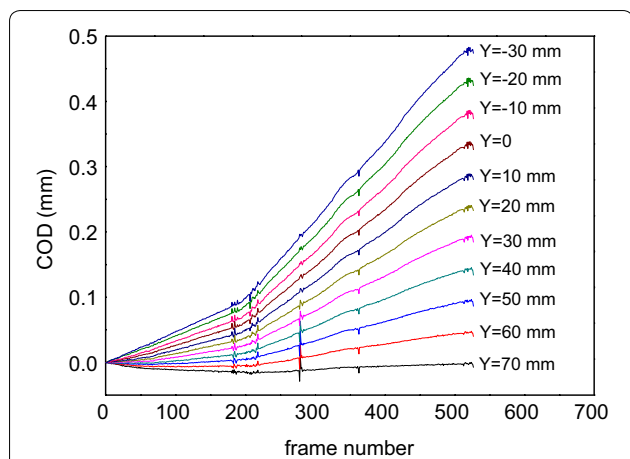


Fig. 10 Variation curves of crack opening displacement in typical sections of Specimen A with loading process under monotonic loading (0.001 mm/s).

than the critical value. But FPZ increases to 25.8 mm rapidly and is 0.37 times of the effective height. Thereafter, FPZ and CTOD continuously propagate with the mechanical loading process. When 16% of the peak load is reached in the post-peak region, CTOD increases to 0.155 mm, approaching the critical value of 0.159 mm, and FPZ reaches its maximum value of 59.94 mm, which is 0.86 times of the effective height. The macrocrack forms when CTOD increases further and exceeds the critical value. At the stage, the length of FPZ decreases rapidly. The determination method of COD curves and FPZs along the whole specimen height in specimen A is shown in Fig. 12. It can be seen from the figure that when the load reaches 15% of the peak load in the post-peak region, the macrocrack propagates forward, and the COD is 0.159 mm at the height of 4.08 mm, which is the starting point of FPZ. The length of FPZ is 58.65 mm, which is 0.84 times of the effective height at this stage. When the specimen is loaded to 10% of the peak load in the post-peak region, the macroscopic crack previously extends to location of 27.54 mm at Y-axis, where the COD is 0.159 mm, as a result, the FPZ length sharply decreases to 36.86 mm, which is 0.53 times of the effective height. When the specimen is loaded to 6% of the peak load in the post-peak region, the macroscopic crack previously extends to location of 34.80 mm at Y-axis, where the COD is 0.159 mm. Therefore, the FPZ length sharply decreases to 29.60 mm, which is 0.42 times of the effective height.

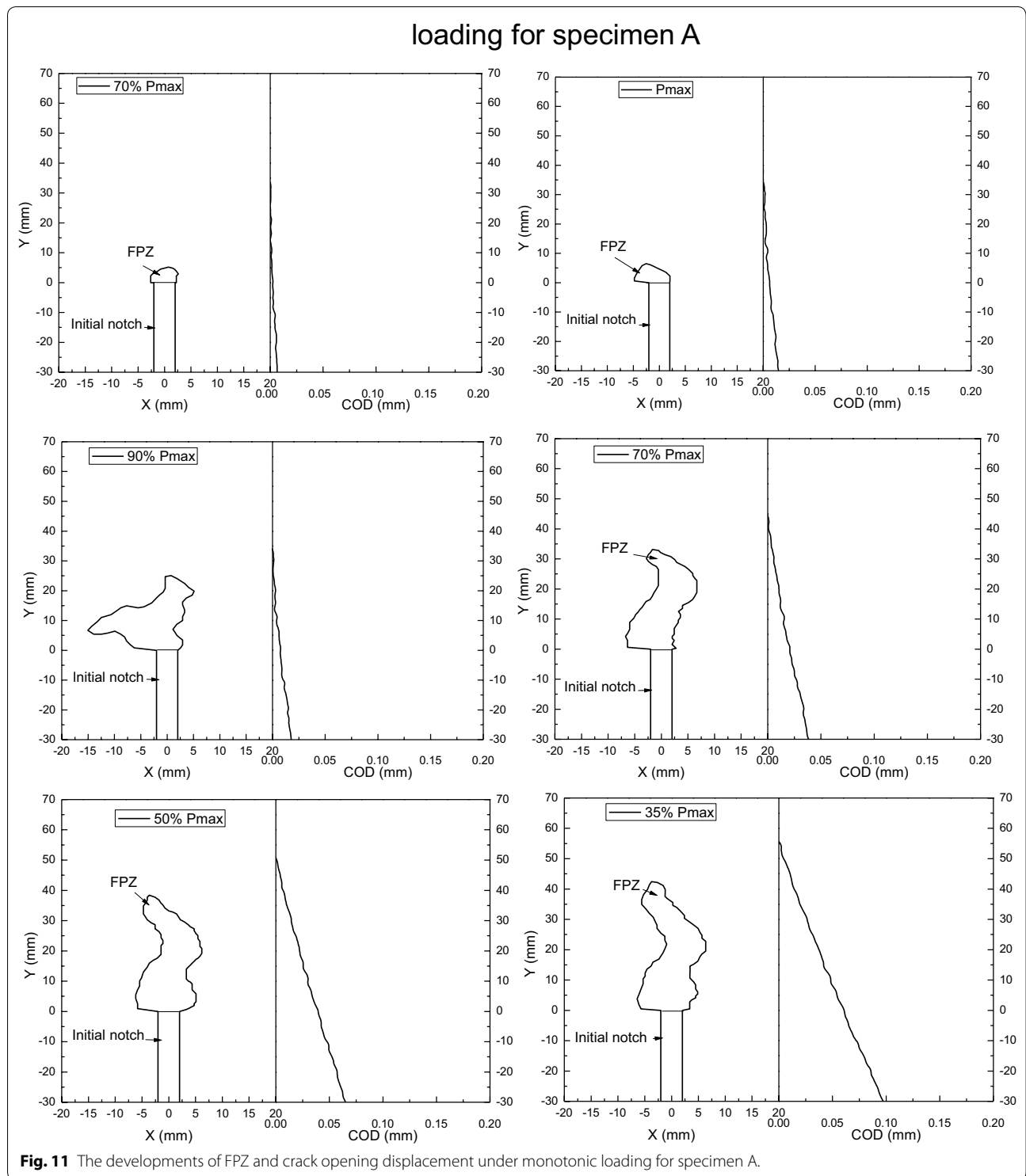
When CTOD exceeds the critical value, a new macrocrack is formed at the front of the initial crack. In order to distinguish FPZ with partial cohesive force, we call the region of the macrocrack as the traction-free zone.

It can be seen from Fig. 12 that the slope of the COD-Y curve decreases significantly after the traction-free zone is formed, especially after the traction free zone develops to a certain extent, e.g. the loading stage of P_{11} . The above phenomenon is consistent with the two-stage process of post-peak softening section, namely the microcrack propagating process (the steep decreasing stage) and the aggregate interlocking process (the gentle decreasing stage). It provides a reliable theoretical basis for describing the mechanism of the softening section of concrete with the bilinear model.

In addition, the propagation speed of the macroscopic crack formed in the traction-free zone is relatively fast at the initial stage. When the load is reduced from 15 to 10% of peak load, the macroscopic crack grows from 4 to 28 mm. When the macroscopic crack continues to grow from 28 to 35 mm, the corresponding load decreases from 10 to 6% of peak load. Although the difference of load change is only 4%, the length of the macroscopic crack changes greatly.

Figure 13 gives the variation of FPZ length l_p with effective crack length a under the strain rate of 0.001 mm/s. It can be seen from the figure that at first FPZ length increases linearly with the increase of effective crack length before stage P_9 . When loading stage P_9 is reached, the FPZ length begins to decrease rapidly in the following loading procedure. That is because that CTOD does not reach the critical value at the initial loading stage and at that time FPZ includes the area from the macro crack tip to the location of the maximum tensile strain. With the mechanical loading procedure, CTOD increases gradually and when it reaches the critical value w_0 , the FPZ length also increases to the maximum value. Specific details are shown in Fig. 13, where the FPZ length is 59.94 mm and the load is 16% P_{max} . Afterwards, as the loading continues, the COD continues to increase, and the new macrocrack begins to propagate forward from the initial crack tip. The propagation speed is much faster than that of FPZ. Therefore, although the effective crack keeps on increasing slowly, the length of FPZ decreases rapidly.

The above phenomenon shows that the development of FPZ of pre-cracked concrete beams under three-point bending loads can be divided into two phases. In the first phase, the crack propagation is prevented by the interlocking between aggregates and microcracks, and the growth speed of COD is comparatively slow. When the other phase (the load is about $1/6 P_{max}$) is reached, the interlocking between aggregates and microcracks gradually decreases until abrupt fracture occurs. At that time, the internal energy is released suddenly and causes the increasing speed of the COD, as well as the growth speed of the macrocrack, which is



consistent with the development trend of the P-CMOD curve obtained by the traditional clip-on extensometer in the previous sections. As a result, the post-peak region of P-CMOD can be divided into two parts. When the load is reduced from P_{max} to $1/6$ of P_{max} , the

first stage is defined, where the curve slope is large, and the COD grows slowly. The other region is the second stage, where the curve slope reduces, but the COD growth speed accelerates. Meanwhile, the development of COD determines the expansion of FPZ.

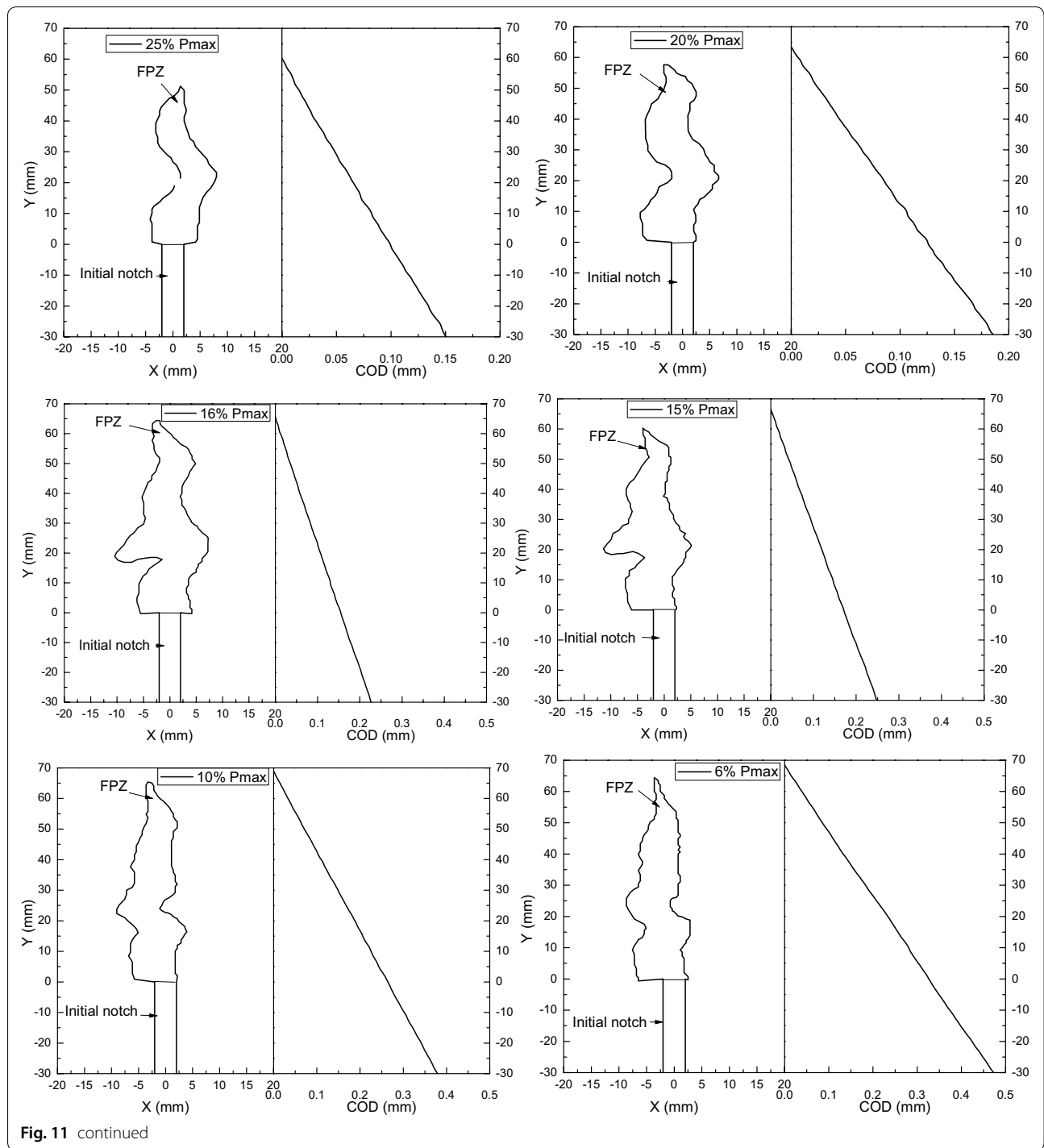
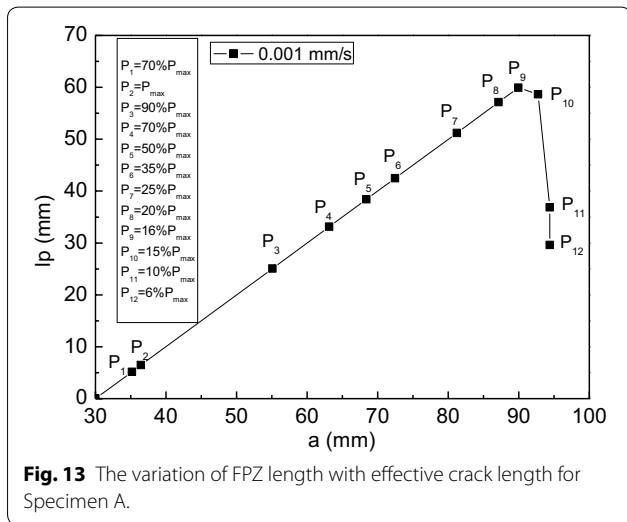
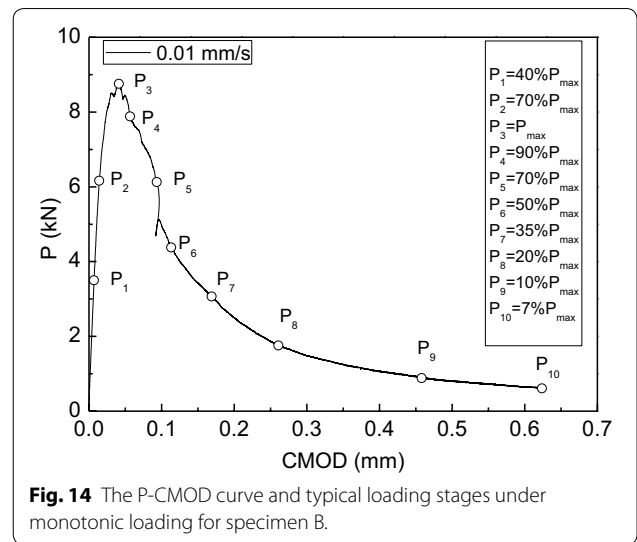
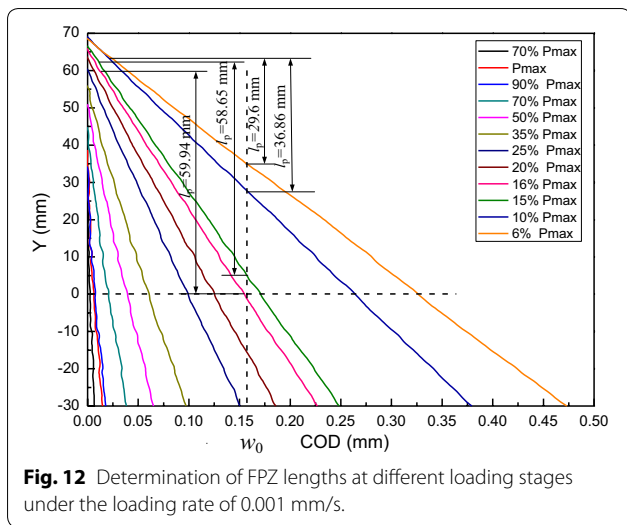


Fig. 11 continued

4.2.2 Specimen B (0.01 mm/s)

The loading rate of 0.01 mm/s in the controlling method of CMOD is used in the monotonic loading of Specimen B and the P-CMOD curve is shown in Fig. 14. To better analyze the fracture procedure of the specimen, 10 typical loading stages are marked in the figure.

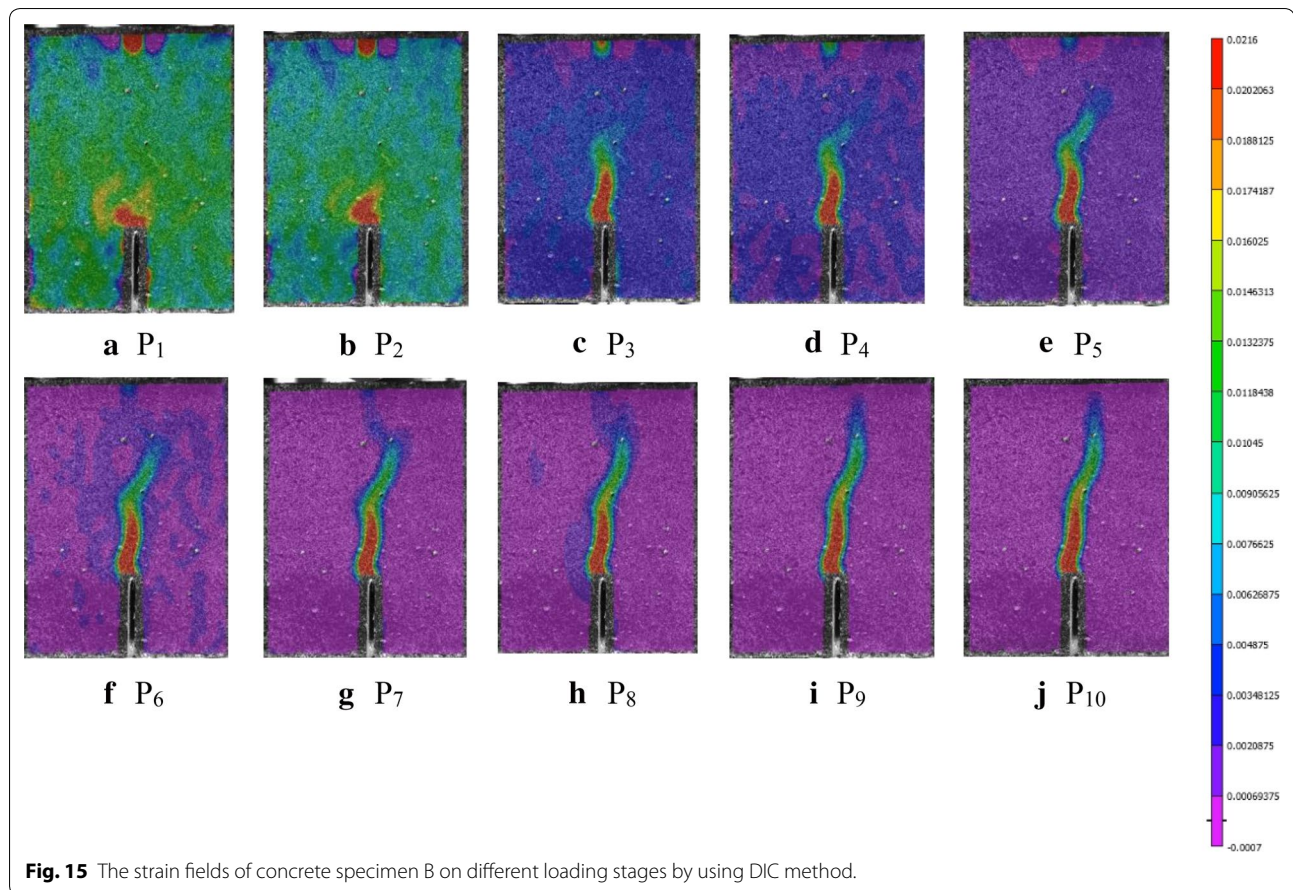
Figure 15 shows the strain field cloud charts of the typical loading stages obtained by DIC method for specimen B. The strain field distribution when the load is smaller than 40% of P_{max} in the pre-peak region is shown in Fig. 15a. It can be seen that although the load is comparatively small and strain concentration region



can be observed at the crack tip, the strain of the measurement areas outside the strain concentration parts is cannot be ignored with the approximate value of 0.010. When P_2 stage is reached, the strain concentration area propagates forward, and the strain of the measurement areas outside the strain concentration parts decreases to around 0.008. When the peak load is reached, a large variation in the strain field can be seen and the strain concentration area grows a lot, forming an obvious crack propagation path. Besides, the strain of the measurement areas outside the strain concentration parts is released and decreases to approximately 0.0034. At the stage of P_4 , strain concentration area continues to propagate and the strain of the measurement areas outside the strain concentration parts is further released,

which is however not so obvious. When the specimen is loaded to stage P_5 , the strain concentration area increases fast while the strain of other areas decreases to about 0.0007, almost in the state of no stress. Finally, in the subsequent loading stages, the strain concentration area continues to develop along crack propagation path, and the strain in other areas is fully released.

Figure 16 shows the FPZs and crack opening displacement distributions of specimen B at the typical loading stages under the loading rate of 0.01 mm /s. When P_1 stage is reached, although a relatively obvious concentration strain area has been formed in the initial crack tip, the CTOD is only 0.01 mm, which is far less than the critical value of full opening. Therefore, only FPZ with length of 5.91 mm can be observed, which is 0.084 times of the effective height. When the specimen is loaded to 70% of the peak value, the CTOD is 0.012 mm and less than the critical value, therefore no macroscopic crack forms. At that time, the length of FPZ is 8.12 mm, which is 0.116 times of the effective height. It can be seen from the shape of FPZs in the previous two stages that the development path is not stable at the initial stage of loading. When the peak load is reached, the CTOD is 0.029 mm and less than its critical value, therefore still no macroscopic cracking occurs. However, the length of FPZ increases rapidly to 32.43 mm and equals to 0.46 times of the effective height. At this point, the length of FPZ has grown to nearly half of the effective height, which gradually makes a clear development path and afterwards FPZ continues to propagate along the path. When loading to 90% of the peak load in the post-peak region, the CTOD increases to 0.039 mm, which still does not reach the critical value, while FPZ grows to 35.19 mm, which is 0.5 times of the effective height. With the continuous



loading process, FPZ continues to propagate and CTOD also keeps on increasing. When 20% of the peak load is reached, CTOD becomes 0.193 mm, exceeding the critical value of 0.187 mm, and a macrocrack emerges at the crack tip. At that time, FPZ reaches the maximum value of 63.92 mm and is equal to 0.91 times of the effective height. At the following stages, CTOD continues to increase with the macrocrack propagating forward and FPZ increasing until the complete failure.

Based on the development of FPZ and crack opening displacement curve above, the FPZ length can be determined. Figure 17 indicates that when the loading rate is 0.01 mm/s, the FPZ length of specimen B changes with the length of the effective crack. It can be seen from the figure that, just as specimen A, CTOD does not reach the critical value at the initial loading stage. At that time, FPZ includes the area from the initial crack tip to the location of the maximum strain and the length of FPZ increases linearly with the increase of the effective crack length. When CTOD increases to the critical value, FPZ is fully developed to the maximum value of 63.92 mm, which is indicated by the point of P_8 in Fig. 17 at about 20% of P_{max} .

4.2.3 Specimen C (0.1 mm/s)

The loading rate of 0.1 mm/s in the controlling method of CMOD is used for specimen C and the P-CMOD curve is shown in Fig. 18. Ten typical loading stages are marked in order for better analysis of the fracture development process. It should be noted that since the loading rate of specimen C is comparatively fast, it is hard to obtain the images of each loading stage even with a high-speed camera. As a result, the corresponding loading stage can only be found on the P-CMOD curve based on typical images those have been taken.

Figure 19 shows the strain field distributions at typical loading stages in Fig. 18 obtained by DIC method for specimen C. On stage P_1 , the strain field distribution before 3% of P_{max} is reached in the pre-peak region can be observed. It can also be seen that the strain concentration areas are not formed at the crack tip due to the small load, but distribute randomly in the entire measurement area, which are mainly caused by initial defects in the specimen. At stage P_2 , a significant strain concentration area forms at the crack tip, and the stress in the measurement areas outside the strain concentration area releases, with the strain quickly dropping to about 0.005. It should

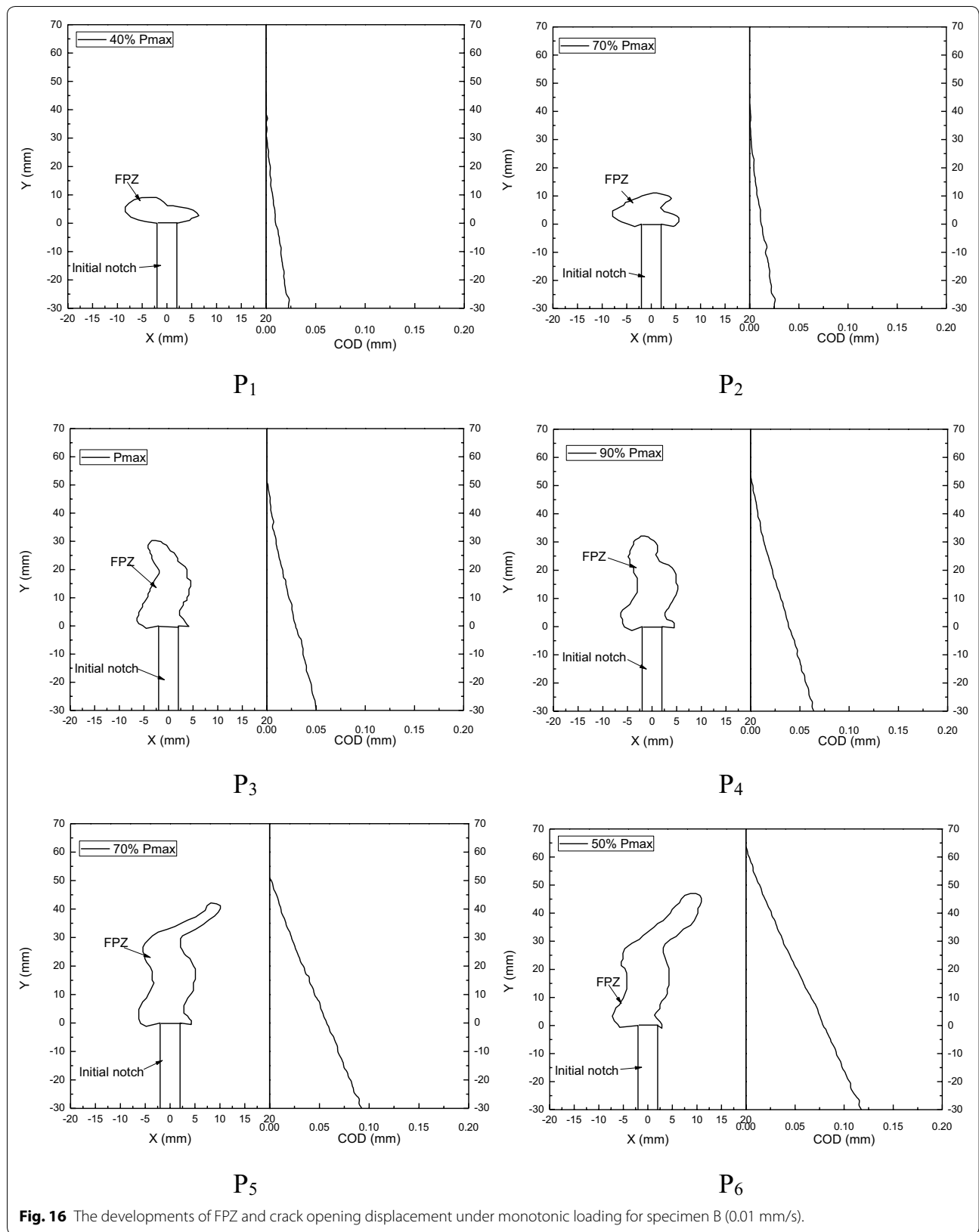
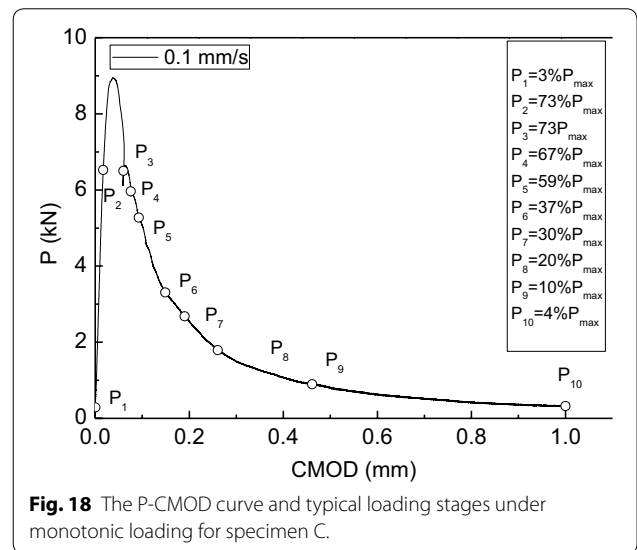
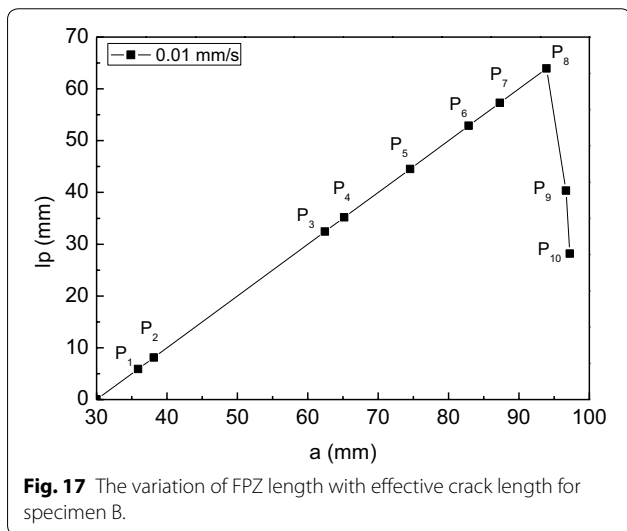
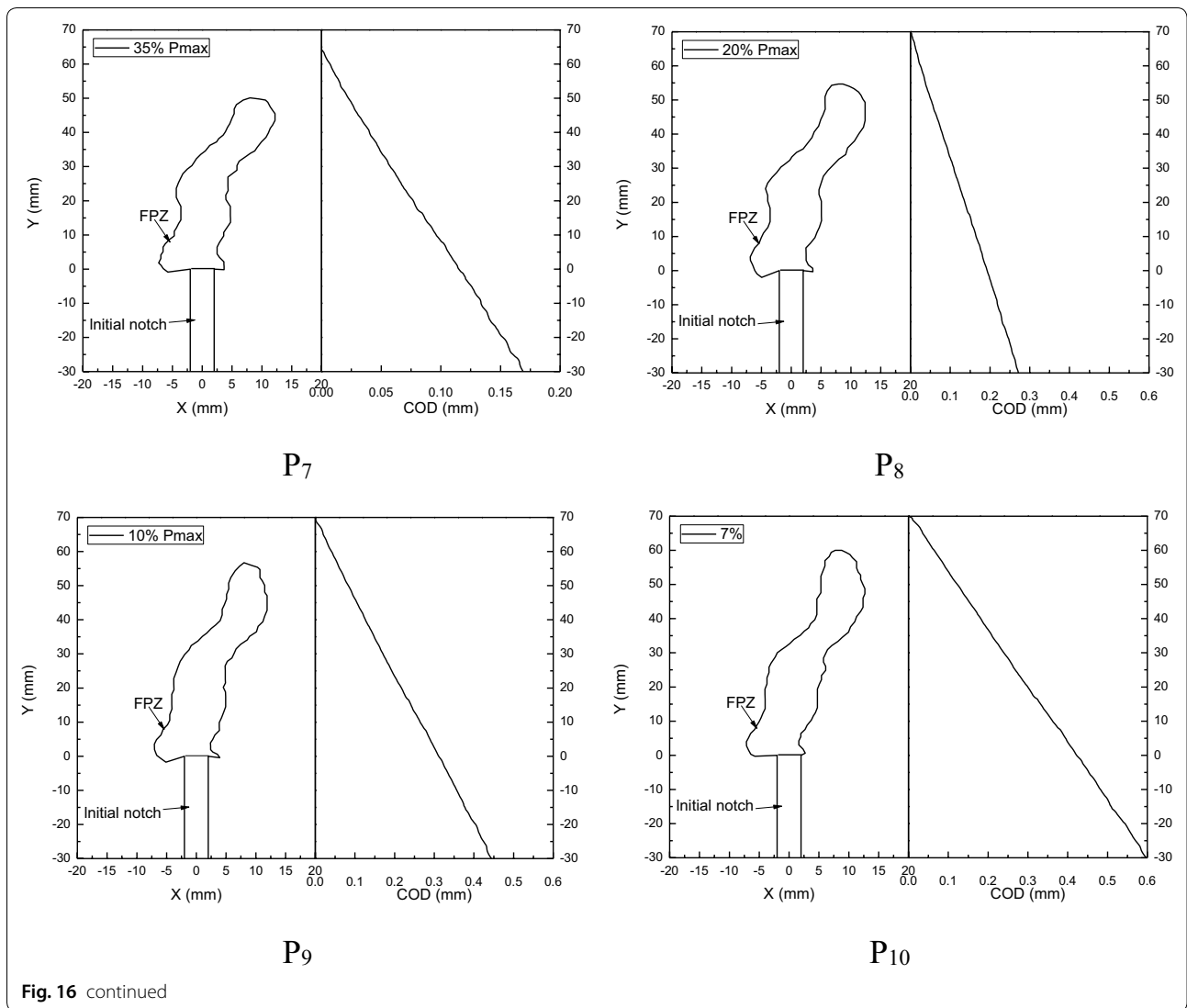
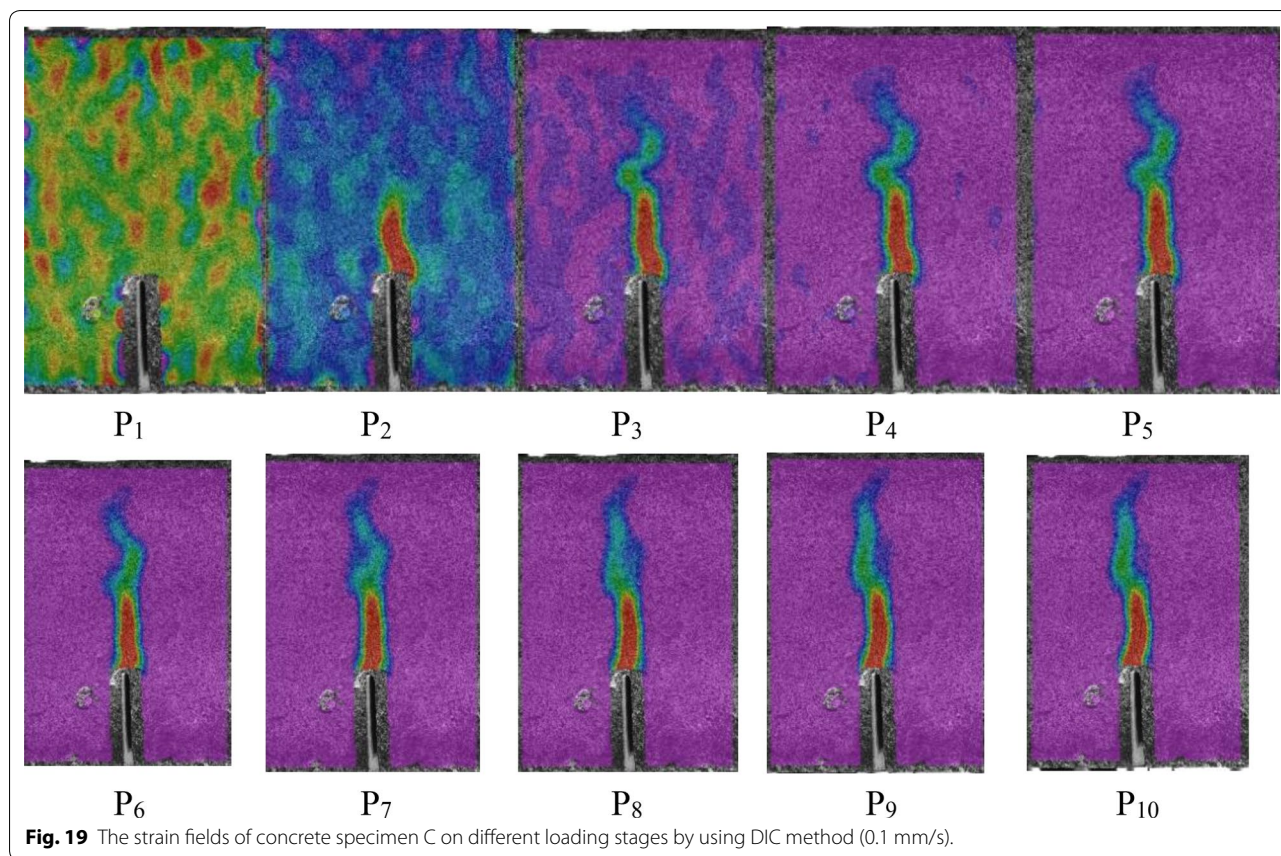


Fig. 16 The developments of FPZ and crack opening displacement under monotonic loading for specimen B (0.01 mm/s).





be noted that due to the fast loading rate, the image is not available at peak load. At the following stage P_3 , where the stress is 73% of P_{max} , the strain field changes and the strain concentration area increases significantly, forming an obvious crack propagation path. Meanwhile, the stress in the measurement areas outside the strain concentration area further releases, with the strain decreasing to about 0.002. At P_4 stage, the strain concentration area continues to increase and the stress almost completely releases outside the strain concentration area. Meanwhile, the crack propagation path is almost completely determined at the stage, after which the strain concentration area continues to develop slowly along the crack propagation path that has formed. What's more, the strain concentration area on the subsequent stages is thin and long, and the strain outside the strain concentration area then completely releases.

Figure 20 exhibits the FPZs and COD distributions of specimen C at typical loading stages under the loading rate of 0.1 mm/s. No strain concentration areas emerge at the crack tip at stage P_1 and the FPZ length can be regarded as 0. At stage P_2 , the FPZ length grows to 25.6 mm rapidly and equals to 0.36 times of the effective height. The CTOD is 0.016 mm and is smaller than the

critical value, therefore no macroscopic cracks forms. It should be noticed that the FPZ length has exceeded one-third of the effective height, which contributes to a clear crack propagation path. At P_3 stage, CTOD increases to 0.055 mm and it is still smaller than the critical value of COD, and no complete cracking occurs. The FPZ length increases to 43.03 mm quickly and is 0.61 times of the effective height. Afterwards, FPZ continues to propagate along the path. At stage P_7 (the load is around 33% of P_{max}), CTOD increases to 0.185 mm, approaching the critical value of 0.187 mm, and a macroscopic crack emerges at the initial crack tip. The FPZ length reaches the maximum value of 59.32 mm and is 0.85 times of the effective height. In the following stages, CTOD further increases with the macroscopic crack and FPZ developing continuously.

Figure 21 shows the variation of FPZ length with effective crack length for specimen C under the loading rate of 0.1 mm/s. Despite the different loading rates, the development law of FPZ with the macroscopic crack is almost the same with those of Specimen A and Specimen B. For Specimen C, the fully developed FPZ length is 59.32 mm with the corresponding stress of 33% of P_{max} in the post-peak region.

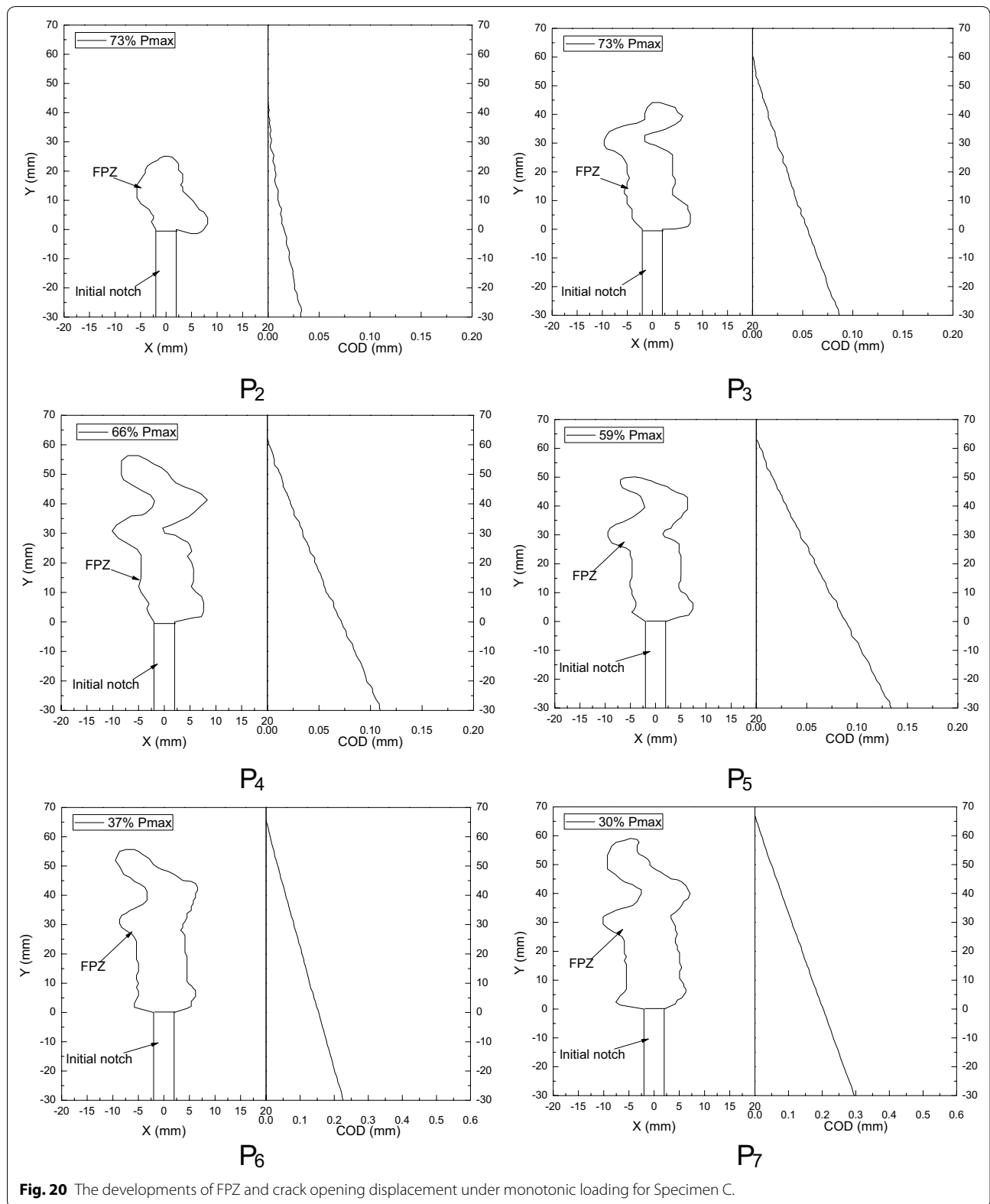
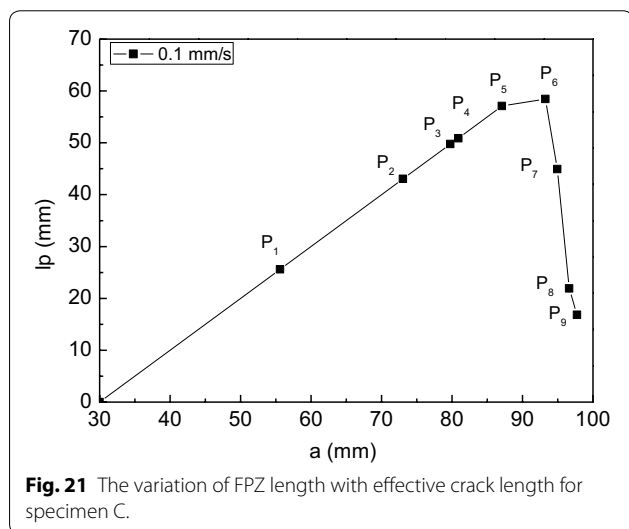
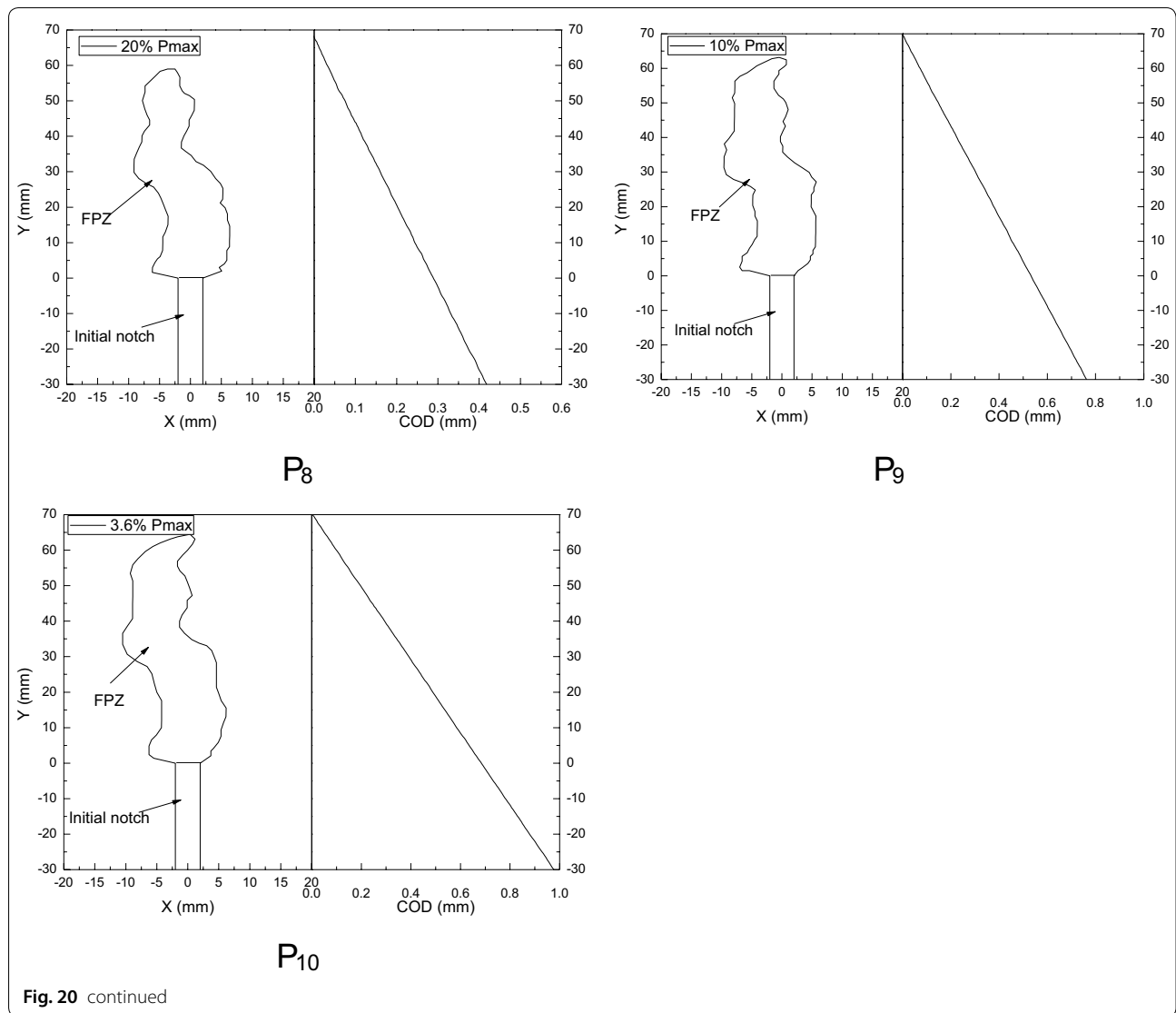
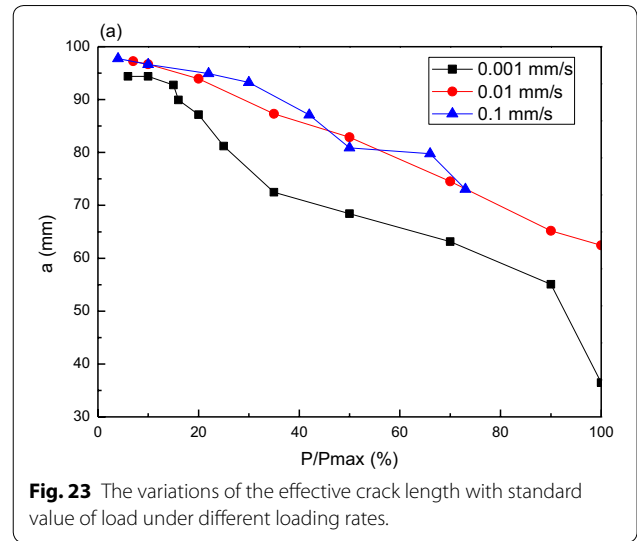
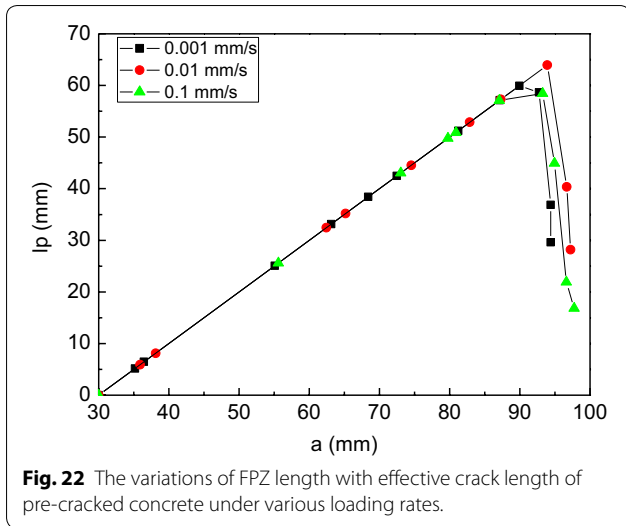


Fig. 20 The developments of FPZ and crack opening displacement under monotonic loading for Specimen C.



4.3 The Influence of Loading Rates on FPZ Length

As a typical quasi-brittle material, concrete is highly influenced by loading rates, which makes it imperative to study the influence of loading rates on the development of concrete FPZ. As a result, monotonic loading conditions with different loading rates of 0.001 mm/s, 0.01 mm/s and 0.1 mm/s are considered in the tests. Figure 22 indicates the variations of FPZ length with effective crack length on these loading conditions. It can be seen that before CTOD reaches the critical value, the length of FPZ increases with the increasing of the effective crack length, which is defined as the sum of the length of the initial crack and FPZ. As loading procedure continues, CTOD keeps on increasing, and when the critical value is reached, the speed of the macrocrack propagation is faster than that of FPZ. Although FPZ length decreases, the total effective crack length still increases slowly. As

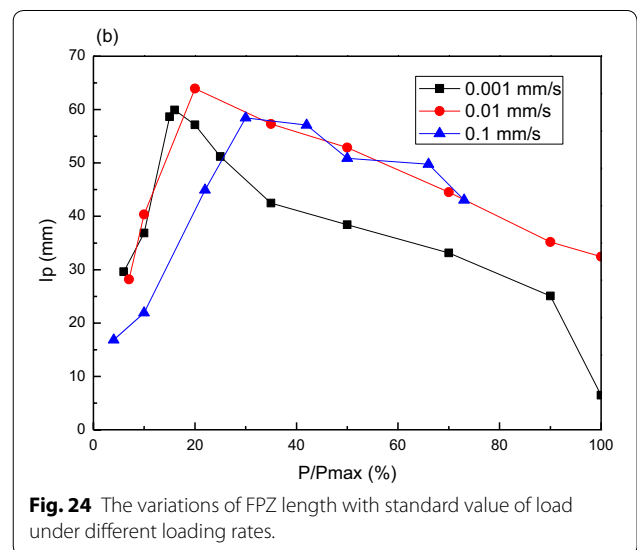


a result, during the entire loading process, FPZ length firstly increases and then decreases with the increasing of the effective crack length. What's more, it can be concluded that a maximum value exists for FPZ length about 60 mm with the corresponding effective crack length of 90 mm. It can be found that there is not obvious influence of loading rates on the maximum value. However, when the specimens fail, the effective crack length increases but the FPZ length decreases with the increasing of the loading rate. It indicates that when the loading rate is faster, not only the effective crack length is larger, but also the proportion of the macroscopic crack increases. The reason for the above phenomenon may be explained by that more cracks in FPZ can fully develop under the slow loading rate. Since cohesive stress exists in FPZ caused by the interlocking of microcracks and aggregates, the cracks in FPZ can develop more sufficiently and makes the macrocrack path develop longer when the loading rate decreases. When the loading rate is fast, there is no enough time for the cracks in FPZ to fully develop. Therefore, the cracks will propagate along the weakest side, which leads to fewer microcracks and the larger macrocrack.

Figure 23 shows the variations of the effective crack length with standard value of load under three different loading rates. This section focuses on the crack propagation law in the post-peak region. It can be seen that the effective crack length increases with the decreasing of the post-peak load. The effective crack length increases with the increasing of loading rate.

Figure 24 shows the variations of FPZ length with standard value of load under different loading rates. Just as the previous section, only the values in post-peak region are studied. It can be seen that the FPZ length

firstly increases and then decreases with the decreasing of load. There is a maximum value of FPZ when it develops sufficiently. Before the maximum value, the length of FPZ decreased with the increasing of loading rate under the same standard value of load. The reason for the above phenomenon may be explained that the faster the loading rate is, the time is not less abundant for FPZ to fully develop, and fewer microcracks form. On this condition, FPZ develops rapidly along the main crack path. The above mechanisms result in that the standard value of load corresponding to the maximum length of FPZ decreases with the increasing of loading rate. After the FPZ length reaches its maximum value, the FPZ length decreases with the decreasing of loading rate under the same standard load. It can be explained that the crack in



FPZ propagates sufficiently under the less loading rate. The FPZ with cohesive stress form a new macroscopic crack in a faster speed and FPZ length decrease instead.

5 FPZ Softening Model

5.1 Softening Model of Concrete

Based on the fictitious crack model, the crack of concrete can be divided into the actual macroscopic crack and the fictitious crack. In the actual macroscopic crack, the crack surface does not transfer any stress. As for the fictitious crack, since the aggregate interlocking can transfer part of the weak cohesive stress, it is assumed by the definition of the fictitious crack. The end of the fictitious crack is connected with the actual crack, where the cohesive stress is 0. Moreover, the tip of the fictitious crack is connected with the undamaged linear elastic part of concrete, where the cohesive stress is equal to the tensile strength of the concrete material. The schematic diagram of mode I crack propagation based on the fictitious crack model is shown in Fig. 25.

It can be seen from the above analysis that DIC method can be used to test the strain field at the crack tip of the pre-cracked concrete beam under the bending load. So that the development and evolution trend of FPZ can be observed intuitively. The cause of the softening properties of concrete is the existence of FPZ because cohesive stress exists between the aggregates in FPZ. The cohesive stress will decrease continuously with the development of the crack until the crack fully develops or the aggregates are pulled out. As a result, the relationship between cohesive stress and COD is the constitutive properties of concrete materials. In the process of the pulling procedure of aggregates or the fracture surface opening, as a result of bonds between fracture surfaces, there is only little deformation in the aggregate bridging interfaces compared with the deformation between the crack surfaces. Therefore, in the post-peak region, CTOD first

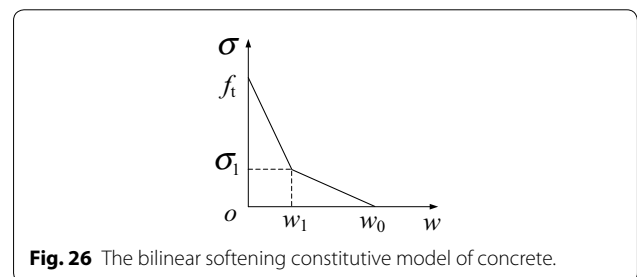
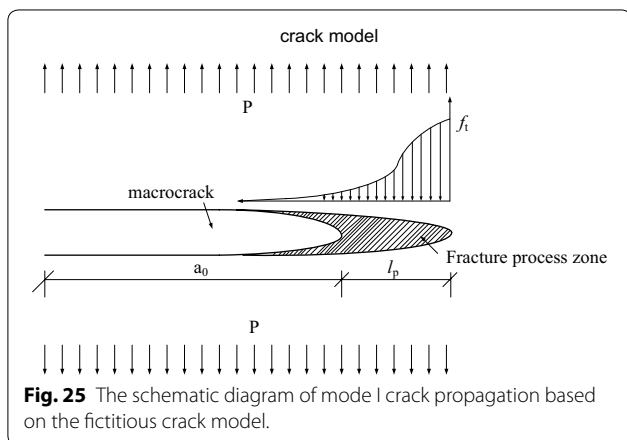
increases slowly and then increases fast abruptly. It may be explained that the interlocking between the aggregates completely breaks and energy is suddenly released. At the same time, a new crack surface forms.

According to the DIC method mentioned in the previous sections, not only the crack propagation of concrete beams during the loading process can be tested, but also the actual macroscopic crack and the fictitious crack can be quantitatively distinguished. Moreover, the P-COD relationship of concrete in FPZ can be determined. In the study, the relationship between the cohesive stress and the COD in FPZ is assumed as bilinear curve as shown in Fig. 26. This model can reflect two most important mechanisms in FPZ, namely, the existence of microcracks and the cohesive stress between aggregates respectively. Therefore, it can be widely applied to the tensile softening constitutive model of concrete (Hillerborg et al. 1976). To be more specific, it is assumed that the steep decrease at the initial softening stage is caused by the microcracks in concrete materials and the plain decrease in the later parts is caused by the interlocking of aggregates in FPZ in the model.

The equations for the bilinear softening model are shown as follows:

$$\begin{cases} \sigma = f_t - (f_t - \sigma_1)w/w_1 & 0 \leq w \leq w_1 \\ \sigma = \sigma_1(w_0 - w)/(w_0 - w_1) & w_1 \leq w \leq w_0 \\ \sigma = 0 & w > w_0 \end{cases} \quad (1)$$

The fracture energy and the tensile strength are both the important parameters in the application of the bilinear softening model. Based on the Hillerborg's model (Hillerborg et al. 1976) mentioned in the previous sections, the parameters of the bilinear softening model for notched concrete beams under three loading rates have been calculated and shown in Table 3. It can be found that the fracture energy and the tensile strength both increase with the increasing of the loading rate. It demonstrates that the concrete material has strain rate effect in softening curve. Since the variations of the parameters of the bilinear model are mainly dependent on the fracture energy and the tensile strength, more attentions should be paid to the relationship between the two parameters



and the loading rate. By linear fitting method, the relationship between the fracture energy, together with the tensile strength, and the loading rate in the range from 0.001 to 0.1 mm/s can be obtained.

$$G_f = 0.028 \log(\dot{w}) + 0.2693, R^2 = 0.96$$

$$f_t = 0.22 \log(\dot{w}) + 4.75, R^2 = 0.94$$

where, G_f and f_t represent the fracture energy (N/mm) and the tensile strength (MPa) of concrete, \dot{w} represents the loading rate (mm/s). Based on the model parameters above, the softening curves of FPZ of concrete under the three different loading rates are shown in Fig. 27. It can be seen that the area enclosed by the softening curve increases, i.e. fracture energy, the tensile strength, and the critical crack opening displacement increase with the increasing of the loading rate. It demonstrates that strain rate effect exists in the tensile softening constitutive relationship in FPZ for concrete materials.

In addition to the parameter determination method proposed in Hillerborg’s model, the CEB-FIP (1990, 2010) also give the respective parameter determination method of the bilinear softening model. Based on the three models, the critical crack opening displacement can be determined by the following equation:

$$w_c = \alpha_F \frac{G_f}{f_t} \tag{2}$$

In different models, the determination of the parameter α_F differs. For Hillerborg’s model, the value of α_F is 3.5. In CEB-FIP (1990), the determination of α_F is dependent on the maximum size of aggregates. When the maximum size of aggregates is 16 mm, the value of α_F is 7, while

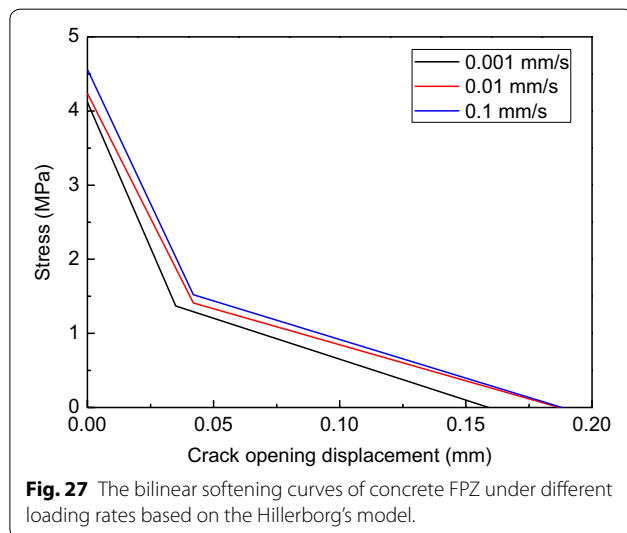
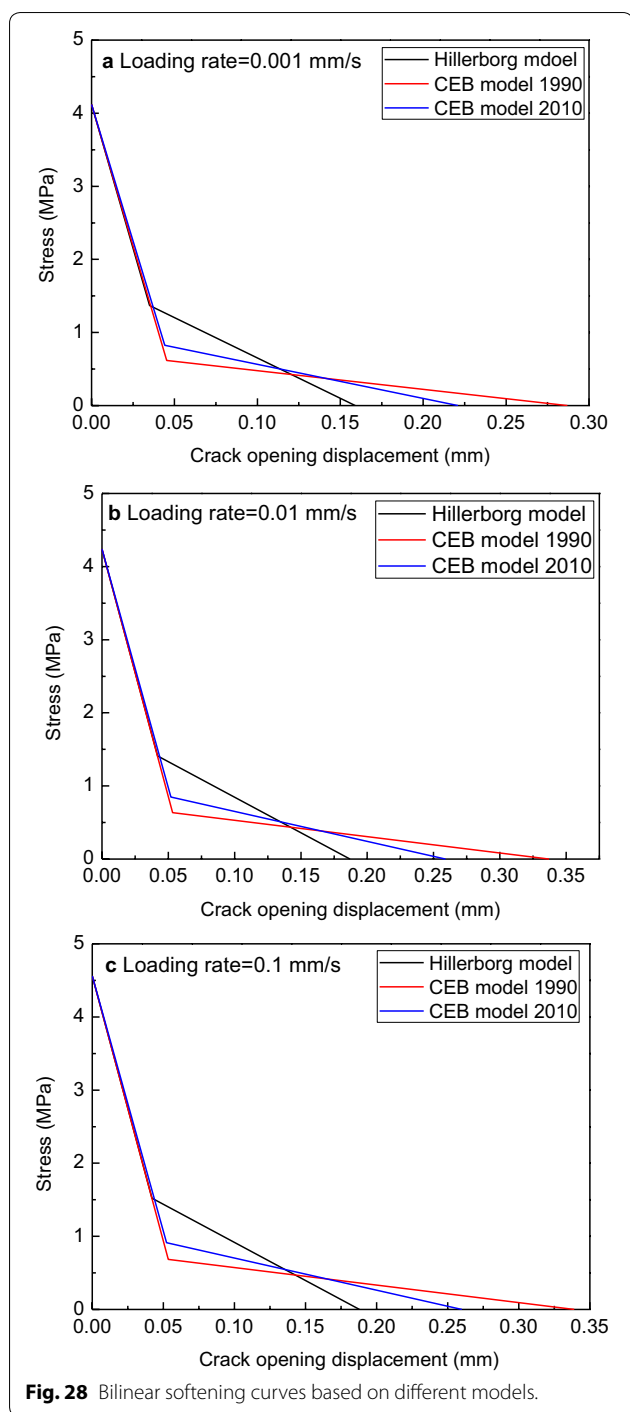


Fig. 27 The bilinear softening curves of concrete FPZ under different loading rates based on the Hillerborg’s model.

when maximum size of aggregates is 32 mm, the value of α_F is 5. Since the maximum size of aggregates in the study is 20 mm, the value of α_F can be calculated as 6.5 based on the interpolation method. In CEB-FIP (2010), the calculation method of the parameter is simplified and the value of α_F is evaluated as 5 no matter what the maximum aggregate size is. The critical crack opening displacement is a threshold value to judge whether the macroscopic crack is formed, which is of great significance to determine the FPZ length. Obviously, the larger the value of the critical crack opening displacement is, the shorter the FPZ length becomes. Since the application of DIC method in this paper can determine the FPZ length more intuitively, it is quite practical to determine the model parameters. In addition to the determination of α_F , the evaluation of the stresses at the turning points in the three models are different. In Hillerborg’s model, the stress at the turning point is suggested as $1/3f_t$. In CEB-FIP models (1990, 2010), the stresses at the turning points are valued as 15% and 20% of the tensile strength of concrete respectively. Since the values of the model parameters are different in the above models, the curve shapes are quite different, which are shown in Fig. 28. It can be seen that the curves of the CEB-FIP model (2010) and Hillerborg’s model are close. While the results of CEB-FIP model (1990) have a large deviation from the calculation results of the other two models. It may be attributed to that the values of the stress and COD at the turning point are larger, while the value of the critical crack opening displacement is smaller. In the future research, a series of concrete fracture tests are still needed to be conducted to provide reliable experimental data for the establishment of more precious concrete softening model.

5.2 Crack Propagation Process

The evolution of FPZ is controlled by CTOD. When CTOD exceeds the critical value, the fictitious crack turns into the macroscopic crack and FPZ continues to develop. Based on the assumption of the bilinear softening curve, FPZ can be divided into four stages, which are shown in Fig. 29. In the figure, a_0 represents the initial crack length, a represents the effective crack length, which consists of the macroscopic crack and the fictitious crack, $\sigma(y)$ represents the cohesive stress, $w(y)$ represents the crack opening displacement, w_1 and σ_1 represent the crack opening displacement and the cohesive stress respectively at the turning point of the bilinear softening curve, f_t and w_0 represent the tensile strength and the critical crack opening displacement of concrete materials, $a(w_0)$ represents the crack length from the location of the crack opening to the location of the crack opening displacement w_0 , $a(w_1)$ represents the crack length



from the location of the crack opening to the location of the crack opening displacement w_1 and the FPZ length is defined as the difference value between a and a_0 .

From Fig. 29a, it can be seen that at the first stage, when the load on concrete specimen is small, the crack opening displacement w_1 is within the range of the

initial crack, and $a(w_1) < a_0$ is valid at that time. Under external loads, FPZ propagates forward. Since CTOD is smaller than w_1 on that condition, the crack opening displacement in the whole process is smaller than w_1 . As a result, it can be inferred from the figure that the cohesive stress is larger than σ_1 and the constitutive relationship of FPZ can be indicated by the first line (the upper part) in the bilinear softening curve. It can also be seen that no macrocracks emerge at the first stage, which corresponds to the linear part of P-CMOD curve of concrete.

With the increase of load, FPZ continues to propagate forward and crack opening displacement keeps on increasing as well. When $a(w_1) > a_0$ and $a(w_0) < a_0$, the point corresponding to the crack opening displacement w_1 is within FPZ, while the critical crack opening displacement occurs in the range of the initial crack. At that time, the development of FPZ goes into the second stage. The range from the location where the crack opening displacement is w_1 to the end of FPZ ($a(w_1) < y < a$) in FPZ is totally within the first line part of the bilinear softening curve. From the initial crack tip to the place where the crack opening displacement is w_1 ($a_0 < y < a(w_1)$), the constitutive relationship of the part can be represented by part of the second line of the bilinear softening model. The second stage corresponds to the nonlinear part in the pre-peak region of P-CMOD curve of concrete, where microcracks aggregates gradually and result in the nonlinearity of P-CMOD curve from the macroscopic perspective.

When the load reaches the maximum value (loading capacity) of concrete specimens, the load gradually decreases with the increasing of the COD and P-CMOD curve enters the softening section. When CTOD increases to w_t ($a(w_0) = a_0$), FPZ comes into the third stage. At that time, the FPZ length is the largest, which is from the macroscopic crack tip to the location where the COD is 0. Since the crack opening displacement of the macroscopic crack tip reaches the critical value, macroscopic crack is always in the critical state of continuous propagation and the cohesive stress in the macroscopic crack decreases to 0. Under this condition, the whole FPZ can be indicated by the entire bilinear softening curve and the stage is in correspondence with the softening part of P-CMOD curve.

On the fourth stage, when the macroscopic crack tip opening displacement exceeds the critical value, the macrocrack propagates forward and the equation $a(w_0) > a_0$ is valid. Under this condition, FPZ starts to decrease and the relationship between the cohesive stress of FPZ and COD can be indicated by the softening constitutive model. The stage corresponds to the stable softening part of P-CMOD curve of concrete.

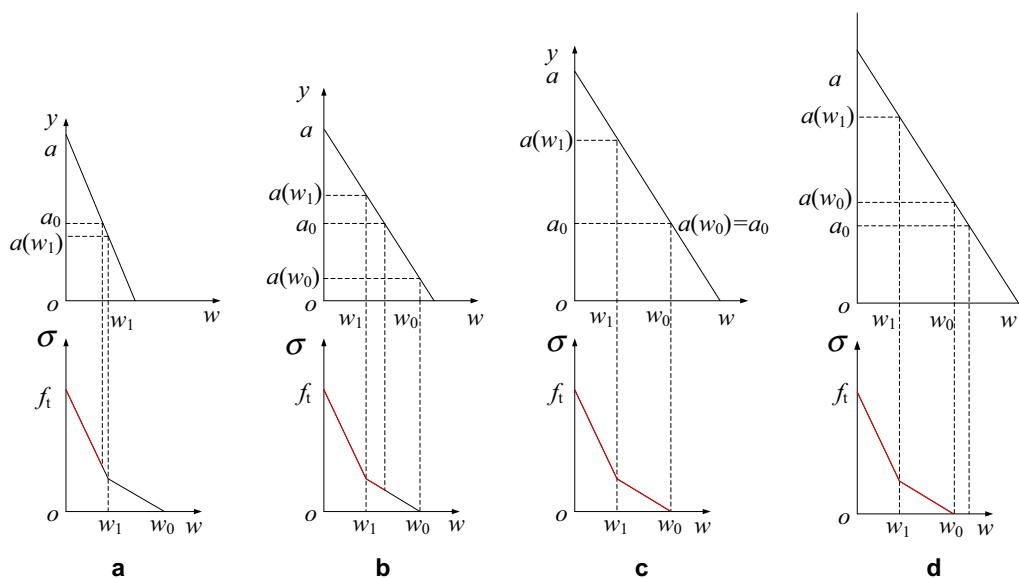


Fig. 29 The schematic diagram of crack propagation at different stages.

6 Conclusions

In this paper, monotonic fracture tests of concrete beams with initial cracks under different loading rates were carried out and DIC method was used to measure the whole field displacement and crack opening displacement of concrete beams. Based on the fictitious crack theory and bilinear softening curve, a softening model of concrete was established with corresponding mechanical properties and propagation law of FPZ quantitatively described and analyzed. The main conclusions can be drawn as follows:

1. As a non-contact nondestructive testing method, DIC technology is feasible in the deformation measurement of concrete materials. The P-CMOD curve obtained by DIC method is almost the same as that measured by the traditional clip-on extensometer. What's more, the shape of P-CTOD curve is in accordance with that of P-CMOD curve obtained by DIC method. However, it can be observed that CTOD is always smaller than CMOD as the different test positions.
2. Based on the assumptions of the fictitious crack model and bilinear softening curve, the authors have proposed softening models of concrete under different loading rates. The tensile strength and fracture energy as the fracture parameters of concrete increase obviously with the increasing of loading rate.
3. The developments of FPZ and the effective crack on different loading stages are obtained by using DIC method. Meanwhile, it is found that FPZ length first

increases and then decreases with the increasing of the effective crack length. FPZ reaches the maximum value of about 60 mm under the three loading rates when the CTOD is equal to the critical crack opening displacement. The load corresponding to the maximum FPZ increases with the increasing of loading rate and the load values are 16%, 20% and 33% of the peak load under the loading rate of 0.001 mm/s, 0.01 mm/s and 0.1 mm/s.

Abbreviations

DIC: Digital image correlation; FPZ: Fracture process zone; COD: Crack opening displacement; CMOD: Crack mouth opening displacement; CTOD: Crack tip opening displacement.

Acknowledgements

This research is based upon work supported by the National Natural Science Foundation of China (Grant No. 51809227) and the Open Foundation of State Key Laboratory of Hydrology-Water Resources and Hydraulic Engineering (Grant No. 2017491711) granted to the first author Jingwu Bu.

Authors' contributions

Monotonic fracture tests on pre-crack concrete beams under various loading rates were carried out. The whole field displacement and crack opening displacement of concrete beams were measured by using DIC method. The lengths of FPZ and effective crack are determined. Based on the fictitious crack theory, a bilinear softening model of concrete was established. All authors read and approved the final manuscript.

Availability of data and materials

The data and material are available.

Ethics approval and consent to participate

The authors state that the research was conducted according to ethical standards.

Consent for publication

The authors consent for publication.

Competing interests

The authors declare that they have no competing interests.

Author details

¹ College of Hydraulic Science and Engineering, Yangzhou University, Yangzhou 225009, People's Republic of China. ² State Key Laboratory of Hydrology-Water Resources and Hydraulic Engineering, Hohai University, Nanjing 210098, People's Republic of China. ³ College of Civil and Transportation Engineering, Hohai University, Nanjing 210098, People's Republic of China.

Received: 14 November 2018 Accepted: 6 March 2020

Published online: 07 May 2020

References

- Al-Osta, M. A., Khan, U., Baluch, M. H., et al. (2018). Effects of variation of axial load on seismic performance of shear deficient RC exterior BCJs. *International Journal of Concrete Structures & Materials*, 12(1), 1–20.
- Ansari, F. (1989). Mechanism of microcrack formation in concrete. *ACI Materials Journal*, 86, 459–464.
- ASTM C33/C33M-18. (2018). *Standard specification for concrete aggregates*. West Conshohocken, PA: ASTM International.
- Bazant, Z. P., & Gettu, R. (1992). Rate effects and load relaxation in static fracture of concrete. *ACI Materials Journal*, 89(5), 456–468.
- CEB-FIP model code. (1990).
- CEB-FIP model code. (2010).
- Chen, X., Xu, L., Liu, Z., & Huang, Y. (2017). Influence of high temperature on post-peak cyclic response of fly ash concrete under direct tension. *Construction & Building Materials*, 154, 399–410.
- Dong, W., Wu, Z., Zhou, X., et al. (2017). FPZ evolution of mixed mode fracture in concrete: Experimental and numerical. *Engineering Failure Analysis*, 75, 54–70.
- Fathima, K. M. P., & Kishen, J. M. C. (2015). A thermodynamic correlation between damage and fracture as applied to concrete fatigue. *Engineering Fracture Mechanics*, 146, 1–20.
- Fu, G., & He, X. (2010). Study on using digital speckle correlation method to test the full-field displacement of concrete surface. *Engineering & Test*, 50(1), 21–23. (in Chinese).
- Gajewski, T., & Garbowski, T. (2014). Calibration of concrete parameters based on digital image correlation and inverse analysis. *Archives of Civil & Mechanical Engineering*, 14(1), 170–180.
- Haneef, T. K., Venkatachalapathy, V., Mukhopadhyay, C. K., et al. (2016). Monitoring damage evolution of concrete prisms under cyclic incremental loading by acoustic emission. *Concrete Research Letters*, 7(2), 43–55.
- Hillerborg, A., Modéer, M., & Petersson, P. E. (1976). Analysis of crack formation and crack growth in concrete by means of fracture mechanics and finite elements. *Cement & Concrete Research*, 6(6), 773–781.
- Hu, S., Zhang, X., & Xu, S. (2015). Effects of loading rates on concrete double-K fracture parameters. *Engineering Fracture Mechanics*, 149, 58–73.
- Huang, C. (2016). *Research on mechanical properties of concrete fracture process zone based on digital image correlation method*. Chongqing: Chongqing Jiaotong University. (in Chinese).
- Krstulovicopara, N. (1993). Fracture process zone presence and behavior in mortar specimens. *ACI Materials Journal*, 90(6), 618–626.
- Lee, J., & Lopez, M. M. (2014). An experimental study on fracture energy of plain concrete. *International Journal of Concrete Structures & Materials*, 8(2), 129–139.
- Meng, W., Yao, Y., Mobasher, B., & Khayat, K. H. (2017). Effects of loading rate and notch-to-depth ratio of notched beams on flexural performance of ultra-high-performance concrete. *Cement and Concrete Composites*, 83, 349–359.
- Otsuka, K., & Date, H. (2000). Fracture process zone in concrete tension specimen. *Engineering Fracture Mechanics*, 65(2), 111–131.
- Peterson, P. E. (1981). Crack growth and development of fracture zone in plain concrete and similar materials. Report No TVBM-1006. Lund Institute of Technology.
- RILEM Draft Recommendation. (1990). Determination of fracture parameter (K_{ics} and CTOD_c) of plain concrete using three point bend tests. *Materials and Structures*, 23, 457–460.
- Rosa, A. L., Yu, R. C., Ruiz, G., et al. (2012). A loading rate dependent cohesive model for concrete fracture. *Engineering Fracture Mechanics*, 82, 195–208.
- Skarzynski, L., Syroka, E., & Tejchman, J. (2011). Measurements and calculations of the width of the fracture process zones on the surface of notched concrete beams. *Strain*, 47(s1), e319–e332.
- Vidya Sagar, R., & Rao, M. V. M. S. (2014). An experimental study on loading rate effect on acoustic emission based b-values related to reinforced concrete fracture. *Construction and Building Materials*, 70(15), 160–472.
- Asmaro, W. P. (2013). *Identification of concrete fracture parameters using digital image correlation and inverse analysis*. Windsor, ON: University of Windsor.
- Wang, C., Xiao, J., & Sun, Z. (2016). Seismic analysis on recycled aggregate concrete frame considering strain rate effect. *International Journal of Concrete Structures & Materials*, 10(3), 307–323.
- Wittmann, F. H., Mihashi, H., & Nomura, N. (1990). Size effect on fracture energy of concrete. *Engineering Fracture Mechanics*, 35(1), 107–115.
- Wu, Z. M., Rong, H., Zheng, J. J., et al. (2011). An experimental investigation on the FPZ properties in concrete using digital image correlation technique. *Engineering Fracture Mechanics*, 78(17), 2978–2990.
- Zhang, X., & Xu, S. (2008). Determination of fracture energy of three-point bending concrete beam using relationship between load and crack-mouth opening displacement. *SHUILIXUEBAO*, 39(6), 714–719. (in Chinese).
- Zhang, X. X., Ruiz, G., & Elazim, A. M. A. (2015). Loading rate effect on crack velocities in steel fiber-reinforced concrete. *International Journal of Impact Engineering*, 76, 60–66.
- Zhu, B. (2011). Numerical simulation on crack propagation of concrete based on extended finite element method. Master thesis, Southeast University. 2011. (in Chinese).

Publisher's Note

Springer Nature remains neutral with regard to jurisdictional claims in published maps and institutional affiliations.